Research

Valosin-containing protein (VCP)–Adaptor Interactions are Exceptionally Dynamic and Subject to Differential Modulation by a VCP Inhibitor*[S]

Liang Xue‡, Emily E. Blythe‡, Elyse C. Freiberger§, Jennifer L. Mamrosh‡, Alexander S. Hebert¶, Justin M. Reitsma‡, Sonja Hess**, Joshua J. Coon§¶‖, and Raymond J. Deshaies‡‡§§

Protein quality control (PQC) plays an important role in stemming neurodegenerative diseases and is essential for the growth of some cancers. Valosin-containing protein (VCP)/p97 plays a pivotal role in multiple PQC pathways by interacting with numerous adaptors that link VCP to specific PQC pathways and substrates and influence the post-translational modification state of substrates. However, our poor understanding of the specificity and architecture of the adaptors, and the dynamic properties of their interactions with VCP hinders our understanding of fundamental features of PQC and how modulation of VCP activity can best be exploited therapeutically. In this study we use multiple mass spectrometry-based proteomic approaches combined with biophysical studies to characterize the interaction of adaptors with VCP. Our results reveal that most VCP-adaptor interactions are characterized by rapid dynamics that in some cases are modulated by the VCP inhibitor NMS873. These findings have significant implications for both the regulation of VCP function and the impact of VCP inhibition on different VCP-adaptor complexes. ***Molecular & Cellular Proteomics 15: 10.1074/mcp.M116.061036, 2970–2986, 2016.***

From the ‡Division of Biology and Biological Engineering, California Institute of Technology, 1200 E. California Blvd, Pasadena, California 91125; §Department of Biomolecular Chemistry, University of Wisconsin-Madison, Madison, Wisconsin 53706; ¶Genome Center of Wisconsin, 425 Henry Mall, Madison, Wisconsin 53706; ‖Department of Chemistry, University of Wisconsin-Madison, Madison, Wisconsin 53706; **Proteome Exploration Laboratory (PEL), Beckman Institute, Division of Biology and Biological Engineering, California Institute of Technology, Pasadena, California 91125; ‡‡Howard Hughes Medical Institute, Pasadena, California 91125

Received May 13, 2016, and in revised form, July 8, 2016
Published, MCP Papers in Press, July 12, 2016, DOI 10.1074/mcp.M116.061036

Author contributions: L.X. and R.J.D. designed research; L.X., E.E.B., E.C.F., and A.S.H. performed research; J.M.R. contributed new reagents or analytic tools; L.X., E.E.B., E.C.F., and J.M. analyzed data; L.X., E.E.B., J.M., and R.J.D. wrote the paper; S.H., J.J.C., and R.J.D. supervised research.

Protein Quality Control (PQC)[1] is thought to play an important role in human health, and mutations in key regulators of PQC lead to neurodegenerative disease (1–4). PQC also is a factor in cancer. During tumorigenesis, many genomic changes occur, including aneuploidy, that place a high demand on cellular mechanisms for coping with proteotoxic stress, including PQC (5–7). The importance of PQC in cancer is highlighted by the use of proteasome inhibitors to treat multiple myeloma (MM) (8, 9). The success of proteasome inhibitors as a therapy for MM has spurred interest in developing a deeper understanding of the significance of PQC to the pathogenesis of cancer, and in identifying other critical mediators of PQC that might serve as alternative targets for therapy of cancer (8).

VCP (also known as p97), a homohexameric AAA ATPase, participates in multiple PQC pathways, including ribosome-, mitochondria-, and endoplasmic reticulum-associated degradation (ERAD)(10–15) and mediates degradation of proteins that misfold because of stress from heat or oxygen radicals (16). VCP also has been implicated in processing of protein aggregates and stress granules via autophagy (17–20). The implication of VCP in PQC mediated by both the ubiquitin proteasome system (UPS) and autophagy suggests that it may serve as a critical node that orchestrates cellular PQC.

The function of VCP is modulated by "primary" binding proteins, of which about two dozen well-validated partners are known (21–23). Of particular interest is a set of adaptors that are thought to serve as specificity factors that link substrates to VCP. These adaptors often contain a VCP interaction motif such as a UBX or PUB domain, and occasionally

[1] The abbreviations used are: PQC, Protein quality control; AP-MS, Affinity purification–mass spectrometry; CX-MS, Cross-linking – Mass spectrometry; ERAD, Endoplasmic reticulum-associated degradation; FDR, False discovery rate; GO, Gene ontology; IP, Immunoprecipitation; LC-MS/MS, Liquid chromatography-tandem mass spectrometry; MAP, Mixing after purification; PAM, Purification after mixing; SEC, Size exclusion chromatography; SILAC, Stable isotope labeling by amino acids in cell culture; UPS, Ubiquitin-proteasome system; VCP, Valosin-containing protein.

contain an ubiquitin-binding domain (24, 25). The N-terminal region (N domain) of VCP can potentially bind 13 different UBX domain adaptors as well as UFD1L-NPLOC4 (24). In several cases, an adaptor plays an important role in linking VCP to a specific substrate, *e.g.* (23, 26–29). However, as a whole the adaptors remain poorly understood. Relatively few adaptor-substrate pairs are known, and in addition little is known about how exactly the adaptors work, including the dynamics of their recruitment and dissociation, and whether these processes are regulated by substrates or other factors. Besides substrate adaptors, VCP also binds enzymes that are thought to act upon VCP substrates. These include ubiquitin chain-extending and chain-trimming enzymes that bind to internal regions on VCP, as well as peptide-N-glycanase which binds near the C terminus (30).

VCP depletion is toxic to cancer cells (31, 32) but is well-tolerated by primary hepatocytes (33) and skeletal muscle *in vivo* (34), suggesting that the VCP network may be a good target for cancer therapy (8). To explore the potential of VCP as a target for cancer therapy, we developed DBeQ and ML240, which are reversible, competitive inhibitors of VCP ATPase activity (31, 35). Subsequent optimization of ML240 yielded CB-5083 (36), which is currently being tested in phase I clinical trials. CB-5083 is a potent inhibitor of the PQC functions of VCP, and as a consequence triggers a massive unfolded protein response that culminates in activation of apoptosis (37). Recently, it was reported that the inhibitory action of ML240 is blunted by the VCP adaptor NSFL1C/p47 (38). This suggests that VCP inhibitors may have selective effects on different complexes, and motivates efforts to better understand the assembly state of VCP in cells, and the impact of VCP inhibitors on its assembly state.

New VCP functions and substrates have been sought through the application of affinity purification-mass spectrometry to identify proteins that bind to either VCP or its adaptors (21, 23, 28, 39). These efforts have identified multiple new functions for VCP, linking it to cullin-RING ubiquitin ligases, endosomal sorting, and ciliary biogenesis. However, this approach is potentially hampered by the dynamics of adaptor-VCP and substrate-adaptor interactions, which remain poorly understood. Here, we take a multi-pronged strategy that combines immunoprecipitation (IP)-mass spectrometry, cross-linking, and size exclusion chromatography -mass spectrometry to study VCP-interacting proteins. These studies revealed that the interaction of VCP with its adaptors is exceptionally dynamic and can be modulated by chemical inhibitors, which we have verified and quantified by direct biophysical studies.

EXPERIMENTAL PROCEDURES

Mammalian Cell Culture—HEK293 cells (ATCC) and BJ fibroblasts were maintained in Dulbecco's Modified Eagle Medium (DMEM) (Sigma-Aldrich, Natick, MA) supplemented with 10% heat inactivated FBS, 100 μg/ml streptomycin, and 100 IU/ml penicillin in 5% CO_2 at 37 °C. Cells were washed with PBS, trypsinized, collected, and frozen at −80 °C for further use.

SILAC Labeling of Cells—For SILAC experiments with HEK293T cells, DMEM lacking arginine and lysine was supplemented with 10% dialyzed fetal bovine serum (FBS), 1% L-glutamine, 1% Pen/Strep, and 1 mM sodium pyruvate. Media used for cells grown in "heavy" was supplemented with 50 mg/L of $^{13}C_6$ $^{15}N_2$-lysine and $^{13}C_6$-arginine (Cambridge Isotope Laboratories, Tewksbury, MA) and 10 mg/L of unlabeled proline, whereas media used for the growth of "light" cells was supplemented with 50 mg/L of unlabeled lysine and arginine and 10 mg/L of proline. Cells were grown in their respective media until incorporation of heavy amino acids reached ~98%, as determined by MS/MS analysis of derivatized amino acid hydrolysate.

CRISPR/Cas9-assisted Chromosomal Knock-in—A donor plasmid (RDB3052) was designed to introduce the FLAG epitope tag sequences into the 5′ end of the VCP coding sequence by homologous recombination. The selection cassette and sequences from the 5′ end of the VCP gene comprising the FLAG sequence flanked by 300 bp upstream and downstream of the VCP initiation codon were connected by the 2A sequence (40). The modified PX330 plasmid (41) (RDB3053) was used to cut the chromosomal VCP locus at the 5′ end of the open reading frame. The CRISPR protocol was then followed (42) and mutant cells were selected for growth in the presence of 100μg/ml Zeocin for 1 week. Surviving colonies were assayed by PCR and Western blotting.

In-cell Cross-linking—In-cell cross-linking was performed using Dithiobis[succinimidyl propionate] (DSP) (Thermo Fisher Scientific, Waltham, MA). For each experiment, DSP was freshly prepared as a 200 mM stock solution in dimethyl sulfoxide (DMSO) and diluted to the appropriate final concentrations in phosphate-buffered saline, pH 7.4 (PBS, Thermo Fisher Scientific). Cells were washed twice with PBS at room temperature to remove residual medium and incubated with DSP for 20 min at room temperature. After removal of the DSP, the cross-linking reaction was quenched by incubating the cells with 25 mM Tris-HCl (pH 7.4) at room temperature for 10 min. The quenching solution was then removed and the cells were frozen and stored at −80 °C.

Experimental Design and Statistical Rationale—SILAC experiment for HEK293 cells treated with NMS873 or MG132 include total four samples. Each SILAC comparison was done in biological duplicate, and then the mass labels were swapped and the experiment repeated in duplicate again. Label free experiment for BJ fibroblast and HEK293 treated with NMS873 or MG132 includes 6 samples in total. Each treatment including control was done separately with biological duplicates. SEC-MS experiment for HEK293 cells treated with NMS873 includes three biological replicates, which contains 16 MS runs each. Two-tailed Student's *t* test was applied to analyze chromatographic peak shift and intensity change. Statistical process for individual experiment would be discussed in following sessions.

Size Exclusion Chromatography for Protein Lysate Fractionation—Cells were collected and lysed by sonication in buffer B (25 mM Tris-HCl pH 7.4, 150 mM NaCl, 1:10000 diluted protease inhibitor mixture (Roche, Basel, Switzerland)) on ice. The chilled lysates were then centrifuged in a SS34 rotor at 13,200 × *g* for 20 min at 4 °C. The cleared supernatant was filtered through a 0.45 μm syringe filter before chromatographic separation. All the samples were normalized based on protein concentration. Size exclusion chromatography was performed on a 24 ml Superose 6 column using an AKTA FPLC system and standard purification templates (GE Healthcare Biosciences, Uppsala, Sweden). The column was equilibrated and then developed in buffer B until the absorption of the flow-through returned to baseline. Sixty fractions of 400 μl each were collected and every third fraction from #11 through #58 was processed for further mass spectrometry analysis.

Protein Digestion of SEC Fractions—Frozen elution fractions from the NMS-873 and VCP knockdown experiments were obtained, along

with wild-type HEK293 fractions prepared alongside each perturbation. Experiments were performed in biological triplicate. To mitigate significant nontryptic peptide activity, urea was added to each fraction prior to thawing for a final concentration of 8 M. Samples were sonicated until urea was completely dissolved, then incubated with 10 mM tris(2-carboxyethyl)phosphine (TCEP) and 40 mM chloroacetamide (CAA) at room temperature for 10 min. Fractions were then pooled by threes, to create 12 final fractions per replicate. Pooled fractions were concentrated on centrifugal filters (Amicon Ultra 0.5 ml Ultracel membrane10 kDa) to ~100 μl. Samples were diluted with 50 mM Tris pH 8 to 1.5 M urea, then digested overnight at room temperature with 3 μg trypsin (Promega, Madison, WI). Samples were acidified with 0.1% trifluoroacetic acid (TFA), then desalted using SepPak C18 solid-phase extraction (SPE) cartridges (Waters, Milford, MA). SPE cartridges were equilibrated with one column volume of 100% acetonitrile (ACN), followed by 0.1% TFA. Acidified samples were loaded on column, followed by washing with three column volumes of 0.1% TFA. Peptides were eluted off the column by the addition of 0.7 ml of 40% ACN with formic acid 0.1% TFA and 0.5 ml 80% ACN with 0.1% TFA. Eluates were dried overnight in a SpeedVac concentrator (Thermo Fisher Scientific), and resuspended in 75 μl of 0.2% formic acid.

Mass Spectrometry Analysis of SEC Fractions—Peptides were injected on to a reverse-phase column prepared in-house. Approximately 35 cm of 75 μm-360 μm inner-outer diameter bare-fused silica capillary, each with a laser pulled electrospray tip, were packed with 1.7 μm diameter, 130 Å pore size, Bridged Ethylene Hybrid (BEH) C18 particles (Waters). Columns were fitted on to a nanoAcquity (Waters) and heated to 55–65 °C using a home-built column heater. Mobile phase buffer A was composed of water and 0.2% formic acid. Mobile phase B was composed of 100% ACN, 0.2% formic acid, and 5% DMSO. Each sample was separated over a 100-min gradient, including time for column re-equilibration. Flow rates were set at 300–350 μl/min.

Peptide cations were converted to gas-phase ions by electrospray ionization and analyzed on a Thermo Orbitrap Fusion (Q-OT-qIT, Thermo). Precursor scans were performed from 300 to 1500 *m/z* at 60K resolution (at 400 *m/z*) using a 5×10^5 AGC target. Precursors selected for tandem MS were isolated at 1 Th with the quadrupole, fragmented by HCD with a normalized collision energy of 30, and analyzed using rapid scan in the ion trap. For some analyses, precursors above 500 *m/z* and signal to noise ratio higher than 1.5 were fragmented by HCD using the described conditions, whereas precursors below 500 *m/z* were fragmented by CAD with a normalized collision energy of 30. The maximum injection time for MS2 analysis was 35 ms, with an AGC target of 10^4. Precursors with a charge state of 2–6 were sampled for MS2. Dynamic exclusion time was set at 15 s, with a 10 ppm tolerance around the selected precursor and its isotopes. Monoisotopic precursor selection was turned on. Analyses were performed in top speed mode with 5 s cycles.

The raw files were searched directly against the *Homo sapiens* database with nonredundant entries (20,198 entries) using Andromeda on Maxquant (Version 1.5.2.8). The proteome database also includes four SEC elution standards (bovine thyroglobulin, bovine γ globulin, chicken ovalbumin, and horse myoglobin). Searches were performed using a precursor search tolerance of 4.5 ppm and a product mass tolerance of 0.35 Da. Search criteria included a static modification of +57.0214 Da on cysteine residues, dynamic modification of +15.9949 Da on oxidized methionine and N-terminal acetylation of + 42.0106 Da. Searches were performed with full tryptic digestion and allowed a maximum of two missed cleavages on peptides analyzed by the sequence database. False discovery rates (FDR) were set to 1% for each analysis.

SEC Chromatogram Analysis—To determine how each treatment (VCP knockdown and incubation with NMS-873) affected how proteins eluted off the SEC column, we calculated an apex shift metric. We are defining "apex" as the fraction in which the majority of the protein elutes. Apex shift was calculated by generating an average fraction number weight against the percent of the total protein that eluted in each fraction. Fractions were numbered 1 through 12, with fraction 1 containing the largest MW proteins/complexes, and fraction 12 containing the smallest. Percent protein per fraction was calculated by first summing the LFQ intensities across the fractions for each protein, then dividing the LFQ intensity in each fraction by the total LFQ intensity in all fractions. The average apex for each protein was then calculated by multiplying each fraction number by the percent protein per fraction, then summing the results. The sum then represents the fraction number in which the majority of the protein elutes, taking into account the spread of the protein across all fractions as well. To calculate average apex shift, we first averaged the apices across biological replicates, then subtracted the mean apex fraction of the wild-type from the mean apex fraction of the corresponding treatment: in doing so, a positive apex shift indicated elution of a protein at a lower molecular weight after treatment than in the wild-type, and a negative shift indicated elution at a higher molecular weight after treatment. *p* values were calculated from the apex fraction numbers across replicates using a two-tailed Student's *t* test. Fold-change calculations were made on total protein across all fractions; LFQ intensities were summed across fractions, $\log_2$ transformed, and averaged, then the mean $\log_2$ intensities from the wild-type samples were subtracted from the mean $\log_2$ intensities in their corresponding treatment samples. *p* values were calculated from the $\log_2$ LFQ intensities across replicates using a two-tailed Student's *t* test.

Western Blotting to Evaluate Fractionation of VCP Adaptors Upon Size Exclusion Chromatography—Samples from cell lysate were prepared by size exclusion chromatography as before, with the addition of 0.05% Triton X-100 in the lysis buffer. Samples were run on a 4–20% gradient SDS-PAGE Gel (Thermo Fisher Scientific), transferred to a nitrocellulose membrane, blocked with 5% milk in TBS-T, incubated with the appropriate primary and secondary antibodies, and developed using Immobilon Western Chemiluminescent HRP Substrate (Millipore) with film. Antibodies used are anti-VCP rabbit polyclonal (Santa Cruz), anti-UBXN7 rabbit polyclonal (EMD Millipore, Billerica, MA), anti-UBXN6 mouse monoclonal (gift from Dale Haines), and anti-UFD1L mouse monoclonal (BD Biosciences), goat anti-rabbit HRP conjugate (Santa Cruz, Biotechnology, Dallas, Texas), and goat anti-mouse HRP conjugate (Santa Cruz, Biotechnology).

Immunoprecipitation/Western Blotting/Mass Spectrometry—Cells were collected and lysed by sonication in buffer A (25 mM Tris-HCl pH 7.4, 150 mM NaCl, 1 mM EDTA, 5% glycerol, 1% Nonidet P-40, and 1× protease inhibitor mixture (Roche)) on ice. Lysates were cleared of debris by centrifugation at 16,000 × *g* for 5 mins and normalized based on protein concentration. One mg of lysate was incubated with 0.2 μl antibodies (Anti-VCP, Abcam ab11433 or Anti-FLAG, Sigma F1804) at 4 °C with rotation for the specified times. The reactions were then supplemented with 20 μl of Protein A/G magnetic beads (Thermo Scientific, 88802) and incubated for 5 min at room temperature. The beads were washed twice with 400 μl of buffer A followed by two washes with 25 mM Tris-HCl pH 7.4. Immunoprecipitates were subsequently processed for Western blotting or mass spectrometry as described below.

To detect immunoprecipitated proteins by Western blotting, bound proteins were eluted by boiling the Protein A/G beads in SDS loading buffer supplemented with 50 mM DTT for 5 min. The eluents were separated on a 10% SDS-polyacrylamide gel and transferred onto a

nitrocellulose membrane. The membranes were probed using antibodies against proteins of interest.

To detect immunoprecipitated proteins by mass spectrometry, a buffer containing 5 mM dithiothreitol, 8 M urea, and 50 mM Tris-HCl, pH 8 was added to the beads. Reduced cysteines were then alkylated by treating the sample with 15 mM iodoacetamide for 30 min. at room temperature, in the dark. After reduction and alkylation, the sample was digested with LysC at a volume ratio of 1:100 (enzyme/sample) for 2 h at room temperature. After LysC digestion, the urea was diluted to 2 M and trypsin was added at a volume ratio of 1:50 (enzyme/sample) and allowed to digest overnight at 25 °C. The next day, tryptic peptides were desalted using a Sep-pak C18 column (Waters) and lyophilized to dryness.

Mass Spectrometric Data Acquisition—Peptide samples were dissolved in 80 μl of 0.2% formic acid and injected into an EASY II nano-UPLC (Thermo Scientific) system. Reverse phase chromatography was performed using a 15 cm silica analytical column with a 75 μm inner diameter packed in-house with reversed phase ReproSil-Pur C_{18}AQ 3 μm resin (Dr Maisch GmbH, Amerbuch-Entringen, Germany). The mobile phase buffer consisted of 0.2% formic acid in mass spectrometry grade water with an eluting buffer of 0.2% formic acid in 80% CH_3CN (Buffer B) run over a linear gradient (8–35% Buffer B, 120 min) and using a flow rate of 350 nL/min. The HPLC system was coupled online with a high-resolution Orbitrap mass spectrometer (LTQ-Orbitrap Elite; Thermo Scientific). The mass spectrometer was operated in the data-dependent mode in which a full-scan MS (from *m/z* 300–1700 with the resolution of 60,000 at *m/z* 400) was followed by 20 MS/MS scans of the most abundant ions using collision-induced dissociation (CID). Ions with a charge state of +1 were excluded and the dynamic exclusion time was set to 60 s after two fragmentations.

Database Search and Quantification—The raw files were searched directly against the *Homo sapiens* database with nonredundant entries (20,198 entries; human Swiss-Prot downloaded on Jan, 2014) using Andromeda on Maxquant (Version 1.5.2.8). Peptide precursor mass tolerance was set to 10 ppm, and MS/MS tolerance was set to 0.8 Da. Search criteria included a static modification of +57.0214 Da on cysteine residues, a dynamic modification of +15.9949 Da on oxidized methionine. Searches were performed with full tryptic digestion and allowed a maximum of two missed cleavages on peptides analyzed by the sequence database. False discovery rates (FDR) were set to 1% for each analysis. For protein-protein interaction analysis, published genetic and physical interactions with VCP were obtained from the BioGRID (43) database, version 3.4.135.

Recombinant Protein Expression and Purification—Full-length VCP was amplified by PCR from human VCP pET15_T(38) and ligated into pET24b using NdeI/SalI to produce a noncleavable C-terminal His-tagged construct (RDB3219). For FRET studies, VCP coding sequences were amplified by PCR and ligated into a modified pET28a vector to produce a construct with a noncleavable C-terminal His-tag and an N-terminal ybbR tag with a short linker (*MDSLEFI-ASKLA*GGGS). Human ND1L (1–480) pET24b construct (RDB2945) is previously described (38). The construct for full-length NSFL1C with a noncleavable N-terminal His-tag (44) was obtained through Addgene (#21268), and site-directed mutagenesis was used to make a NSFL1C-Thr370Cys mutation. Proteins were expressed and purified as described previously (38), with the exception that NSFL1C was expressed in TOP10 cells for 3 h at 37 °C. For FRET, NSFL1C-Thr370Cys was incubated with tetramethylrhodamine-5-maleimide (ThermoFisher) prior to gel filtration to produce $NSFL1C^{TAMRA}$. For ybbR labeling, Cy5-CoA conjugate and Sfp enzyme were made as described (45). Thirty micromolar ybbR-VCP was incubated for at least 3 h at room temperature with 60 μM Cy5-CoA conjugate and 12 μM Sfp in 50 mM HEPES pH 7.4, 10 mM $MgCl_2$ prior to gel filtration. All proteins were purified on a Superose 6 gel filtration column.

FRET Measurements—All FRET measurements were carried out in 20 mM HEPES, pH 7.4, 100 mM KCl, 3 mM $MgCl_2$, 1 mM TCEP, and 1 mg/ml ovalbumin (Sigma). Nucleotides were optionally present at 2 mM, and inhibitors were optionally present at 15 μM. Equilibrium binding assays were carried out on a FluoroLog-3 (Jobin Yvon), with excitation at 540 nm and emission scan 555–750 nm. Stopped-flow experiments were carried out on a Kintek SF-300X instrument with excitation at 540 nm and a 580/20 emission filter. Data were analyzed using Prism 6 (GraphPad).

RESULTS

Study of VCP Complex Assembly Using Size Exclusion Chromatography-mass Spectrometry—To investigate VCP's association with its adaptors and other binding partners, we sought to employ size exclusion chromatography (SEC) in a buffer containing no detergent and low salt, with the idea that gentle conditions might preserve the integrity of native protein complexes. For these experiments, we prepared lysates from HEK293 cells that were untreated, supplemented with NMS873 for 6 h, or depleted of VCP by doxycycline induction of shRNA (supplemental Fig. S1*A*). The lysates were fractionated on a gel filtration column, and every third fraction was analyzed by shotgun mass spectrometry.

To evaluate the fractionation behavior of the 7919 proteins identified in three biological replicates of both the control *versus* NMS873-treated or control *versus* VCP knock-down experiments, we developed an algorithm that estimated the relative amount of each protein by label-free quantification, as well as the mean fractionation position (apex) on the size exclusion column. A histogram summarizing the apex shifts for all proteins identified in the perturbation experiments as well as an untreated *versus* untreated control is shown in Fig. 1*A*. The variability in the fractionation behavior of known VCP adaptors, number of identified proteins in each experiment, and changes in protein level observed upon depletion or inhibition of VCP are plotted in supplemental Figs. S1*B*–S1*D*. The fractionation behavior of all ~8000 proteins is consolidated in supplemental Table S1 and fully listed in supplemental Table S2.

We observed that for both NMS873 treatment and VCP knockdown, there was a bias for proteins increasing in molecular weight (*i.e.* eluting in any earlier fraction, possibly because of accumulation in larger protein complexes) and decreasing in abundance, with the bias being stronger for the former (Fig. 1*B*, 1*C*). The known functions of VCP in protein complex disassembly (12, 13) suggested we might observe a bias for proteins increasing in molecular weight and abundance following VCP inhibition, as these proteins would remain trapped in complexes (including complexes with VCP in the case of NMS873 treatment) and unavailable to the proteasome for degradation. Some of these proteins may associate with membranes, chromatin, or other sedimentable structures, which, given that our lysis buffer did not include detergent or nucleases, could explain their unexpected ap-

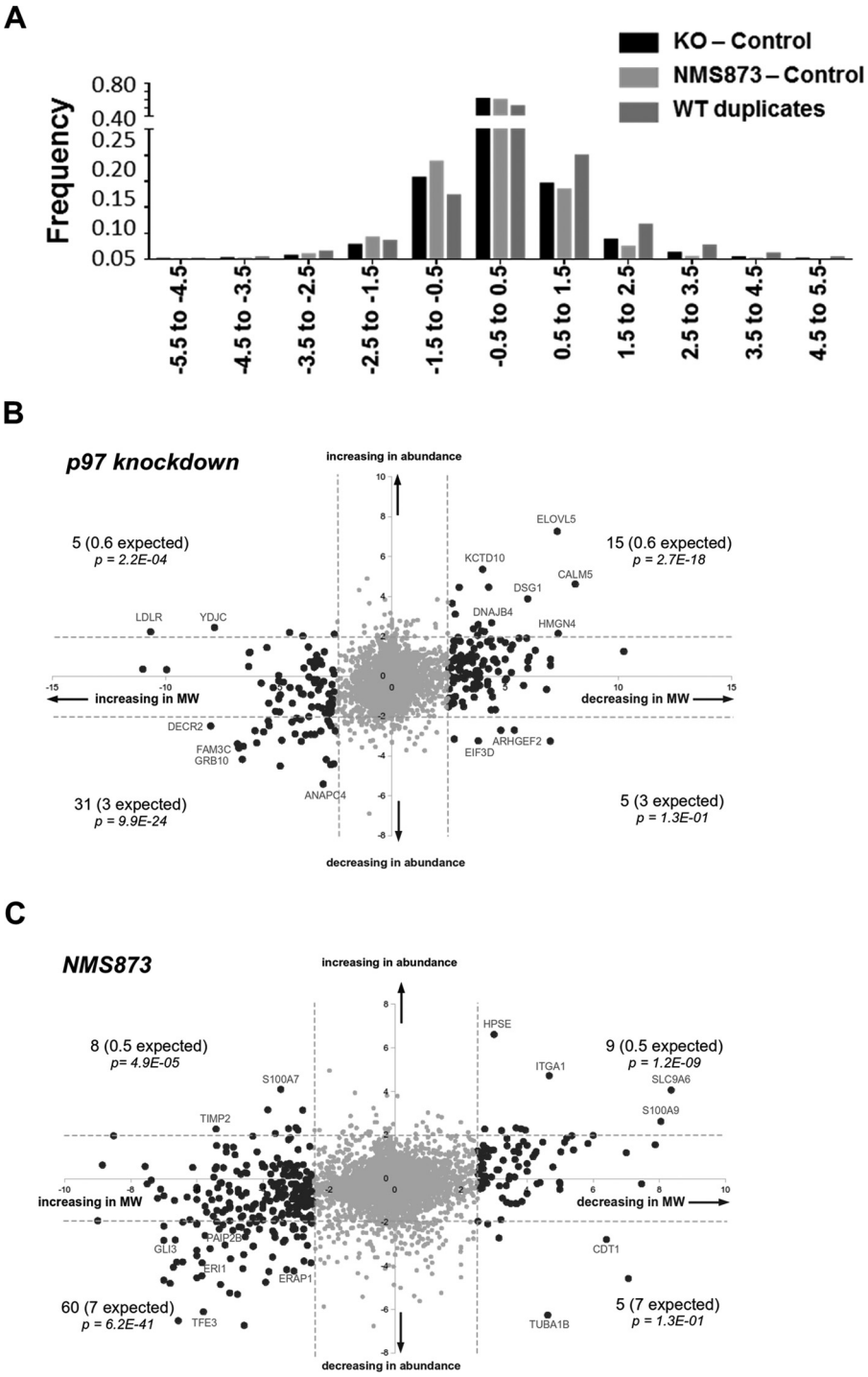

FIG. 1. **Analysis of the fractionation behavior of cellular proteins by SEC-mass spectrometry in response to modulation of VCP activity.** HEK293 cell lysate from untreated or perturbed cells was chromatographed on a Superose-6 column, and every third fraction was subjected to shotgun sequencing by mass spectrometry. *A*, Histogram of apex shifts of proteins in treated cells relative to control cells ($A_{treated} - A_{control}$) for all 7919 proteins identified in the SEC-MS analysis. The apex for each protein is defined as the fraction in which the protein is present in the highest amount. Plotted data are the average of triplicates. *B*, Molecular weight shift and abundance fold change (log scale) in response to VCP knockdown compared with control knockdown. Proteins in area that is not grayed out represent those with >2.5 mean apex shift. Of these proteins, enrichment for a > fourfold change in abundance (those above or below the horizontal dotted lines), relative to all proteins identified by SEC-MS, was calculated. The average values of triplicate measurements are reported. *C*, Same as panel *B*, except that cells were mock-treated or treated with 10 μM NMS873 for 6h.

parent decrease in abundance. Proteins that shifted in molecular weight in response to VCP inhibition do not share biological functions (supplemental Fig. S1*E*). Few of the proteins we identified as changing in molecular weight and abundance following VCP modulation had been previously reported as VCP-associated (supplemental Fig. S1*F*, S1*G*). The proteome elution pattern in our SEC experiments generally agrees with a previous data set generated by Kirkwood and coworkers (46).

Using the data set in supplemental Table S1, we generated theoretical chromatograms for VCP and a subset of its adaptors. For this investigation we focused on UFD1L-NPLOC4 and the putative substrate-recruiting UBX domain adaptors that bind the N-terminal domain, of which 12 were identified (theoretical chromatograms for these proteins are shown in Figs. 2*A*–2*D* and supplemental Figs. S2*A*–S2*C* and the reproducibility of their fractionation across triplicates is shown in

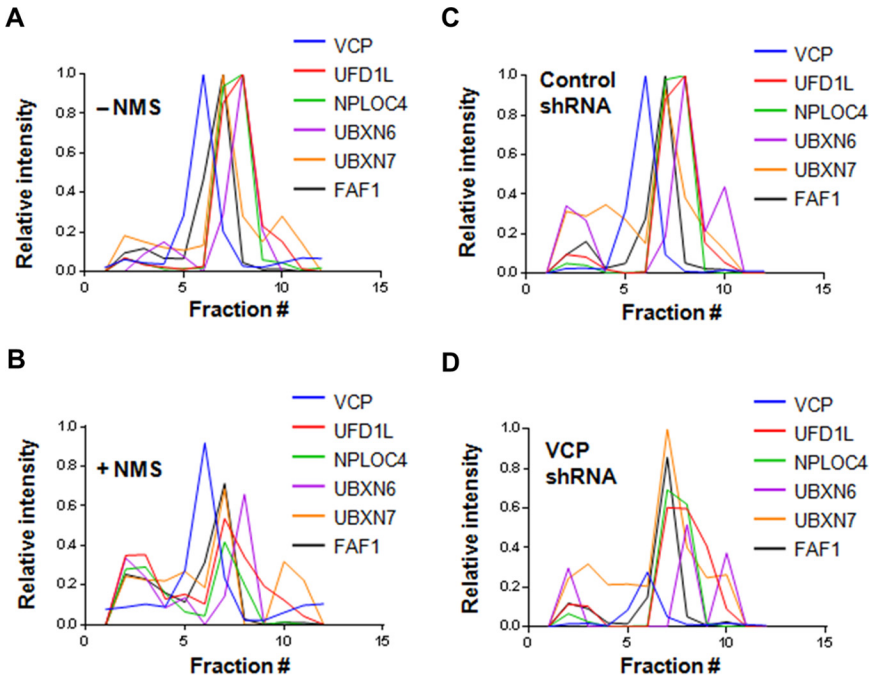

FIG. 2. **Analysis of the fractionation behavior of VCP and its adaptors by SEC-mass spectrometry in response to modulation of VCP activity.** *A*, The relative LFQ intensity of peptides from VCP and Class IV adaptors in SEC fractions from untreated HEK293 cells were averaged to generate an estimate of the level of these proteins in each fraction. These levels were then plotted. Quantitative data on the behavior of triplicates for each protein are provided in supplemental Fig. S2*D*. *B*, same as panel *A*, except that cells were treated with 10 μM NMS873 for 6 h prior to lysis. *C*, Same as panel *A*, except that cells were transfected with control shRNA 96 h prior to lysis. *D*, Same as panel *A*, except that cells were transfected with shRNA against VCP sequences 96 h prior to lysis.

supplemental Fig. S2*D*). Evaluation of their fractionation behavior in untreated *versus* perturbed cells revealed that they could be segregated into four distinct classes as follows.

Class I adaptors, comprising UBXN2A and ASPSCR1, exhibited strong cofractionation with VCP in untreated cells, and were not affected by NMS873 treatment (supplemental Fig. S2*A*). Class I adaptors appear to have a more stable association with VCP than other adaptors. Moreover, UBXN2A levels were reduced below detection upon VCP depletion (supplemental Fig. S2*A*), suggesting that its stability was dependent upon assembly with VCP. ASPSCR1 was not affected by VCP depletion, but it should be noted that only 80% depletion of VCP was achieved and thus VCP may still have been present in sufficient amounts to saturate ASPSCR1.

UBXN4, UBXN8, and FAF2 define Class II VCP adaptors, which were constitutively assembled in complexes of higher MW than the VCP peak regardless of whether or not VCP was depleted or inhibited with NMS873 (supplemental Fig. S2*B*; note that UBXN8 was not detected in the experiment with VCP-depleted cells). Thus, the high MW forms of these proteins presumably arose from assembly with proteins other than VCP. Interestingly, UBXN4 and UBXN8 are ER membrane proteins, yet our analysis was performed on cell lysates prepared without detergent. It is not known whether the forms of UBXN4/8 detected here are in small vesicles or are proteolytic fragments released from the ER.

The Class III adaptors UBXN2B, NSFL1C, and UBXN1, migrated at MWs lower than the VCP peak, and were not affected by either chemical inhibition or depletion of VCP (supplemental Fig. S2*C*).

The Class IV adaptors UFD1L, NPLOC4, UBXN7, and FAF1 migrated primarily at MWs lower than the VCP peak in unperturbed cells (Fig. 2*A*), but a substantial fraction of each was recruited into high MW complexes upon inhibition of VCP with NMS873 (Fig. 2*B*). Formation of these higher MW complexes was not an indirect consequence of a reduction of VCP activity, because a similar shift in MW was not observed in cells depleted of VCP (Fig. 2*C*, 2*D*). This suggests that NMS873 stabilized formation of high MW complexes between these adaptors and VCP.

The only adaptor that did not fit neatly into Classes I-IV is UBXN6. In the presence of NMS873, UBXN6 shifted to higher MW like UBXN7, but in the depletion experiment it partitioned into high and low MW complexes (Fig. 2*A*–2*D*). We note that the theoretical chromatograms for VCP, UBXN6, UBXN7, and UFD1L match the fractionation of these proteins as determined by Western blotting of SEC fractions (supplemental Fig. S2*E*). We also note that retrospective analysis of theoretical chromatograms derived from a data set generated by Kirkwood *et al.* (46) (supplemental Fig. S2*F*) yielded results for unperturbed cells similar to ours with the exception of UBXN6, which exhibited a high MW peak in our data set but not theirs, and UBXN4 and UBXN8, which were not detected in their data set, most likely because they did not analyze very high MW fractions (*e.g.* as shown in supplemental Fig. S2*F* Kirkwood *et al.* did not capture the entire VCP peak, whereas we did, as shown in supplemental Figs. S2*A*–S2*C*).

VCP-adaptor Interactions Are Exceptionally Dynamic—The results of the SEC-mass spectrometry took us by surprise, because even well-studied adaptors like UFD1L-NPLOC4, UBXN7, and NSFL1C showed little or no cofractionation with VCP in unperturbed cells. This suggested to us that VCP might exhibit much more dynamic association with its adaptors than was previously appreciated. To address this ques-

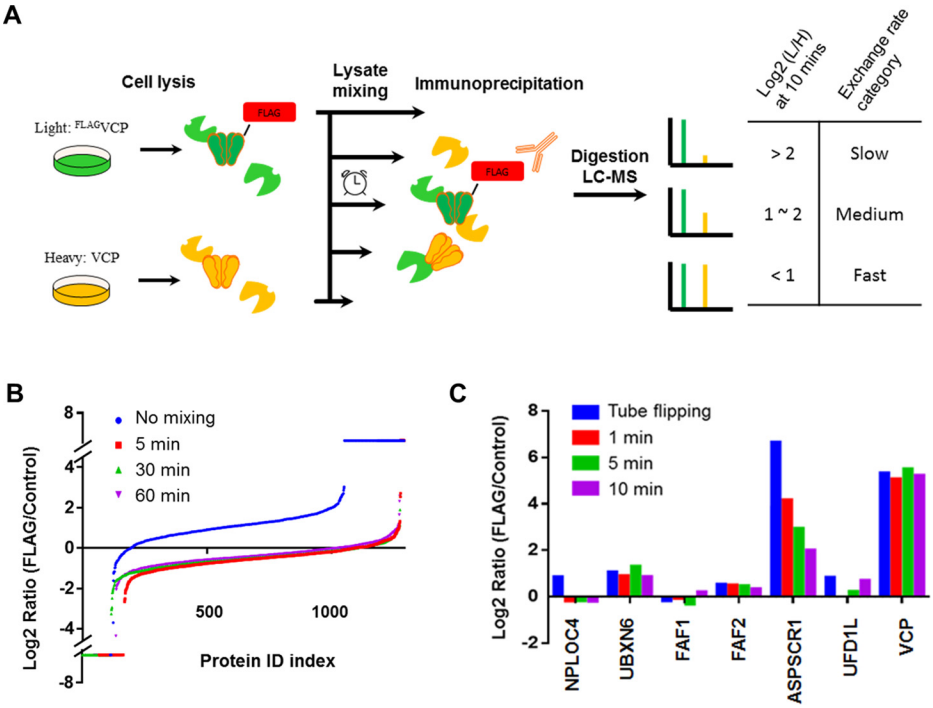

FIG. 3. **VCP-adaptor complexes undergo rapid exchange during IP from cell lysate.** *A*, Schematic workflow of IP-MS experiment for studying VCP adaptor exchange. *B*, Global protein exchange during IP. HEK293^{FLAGVCP} and HEK293 cells were grown in medium containing "heavy" or "light" lysine plus arginine, respectively. The cell lysates were mixed and incubated with anti-FLAG antibody for the indicated amount of time prior to collecting immune complexes on protein A/G resin for 5 min. For "No mixing", samples were mixed after the IP step. $n = 1$ for all treatments. *C*, A repeat of the experiment in *B*, except that shorter IP times were evaluated and the antibody capture interval was reduced to 1 min. "Tube flipping" corresponds to five inversions of the capped tube. H/L ratios are reported for VCP and the indicated adaptor proteins. $n = 1$ for all treatments.

tion, we performed conventional affinity purification-mass spectrometry experiments. The first approach we took was to immunoprecipitate VCP from HEK293 cell lines in which the genomic locus of VCP was modified using CRISPR/Cas9 technology (47) to encode VCP with a FLAG epitope appended to its N terminus (HEK293^{FLAGVCP} cells). Although we successfully obtained cell lines that expressed endogenous VCP bearing an N-terminal FLAG tag (^{FLAG}VCP, supplemental Fig. S3*A*), we were unable to obtain cell lines in which all alleles of VCP were tagged, suggesting that this might be a lethal event.

Shotgun mass spectrometry following immunoprecipitation (IP) of endogenous ^{FLAG}VCP retrieved with anti-FLAG resin consistently yielded hundreds of proteins. To determine how many of these proteins were likely to be specific VCP binding partners as opposed to nonspecific contaminants, we performed a control experiment in which lysate from HEK293^{FLAGVCP} cells grown in medium containing heavy lysine and arginine was mixed with lysate from untagged HEK293 cells grown with light lysine and arginine (referred to here as a purification after mixing (PAM)-SILAC protocol) (48). Anti-FLAG IP for 60 min followed by mass spectrometry revealed that a large fraction of the identified proteins had $\log_2$ H/L ratios between −1 and 1 (supplemental Table S3), which is a range that many false positives fall in because of analytical error (49). However, given the poor cofractionation of adaptors observed in the SEC-mass spectrometry experiments as well as results from unrelated studies in which we observed a remarkable level of exchange of F-box proteins during IP of Cul1 (J.M.R., unpublished data), we wondered whether the small number of proteins with H/L $\log_2$ ratios >1 might be because of exceptionally dynamic association of VCP with its physiological partners. To assess this possibility, we repeated the analysis, but in this case we performed a mixing after purification (MAP)-SILAC experiment (48) in which tagged heavy and untagged light samples were subjected to IP separately and then mixed immediately before LC-MS/MS analysis (Fig. 3*A*). This revealed that a large fraction of the proteins identified in the IP from HEK293^{FLAGVCP} lysate had a H/L ratio >1 and thus were enriched relative to the IP from lysate of control cells. Reducing the IP duration from 60 min to 30 or even 5 min in the PAM-SILAC protocol modestly reduced the recovery of ^{FLAG}VCP and adaptors (supplemental Fig. S3*B*, S3*C*), but did not significantly attenuate exchange (Fig. 3*B*, supplemental Table S3).

To investigate this further, we repeated the experiment but with shorter IP intervals ranging from 10 min down to the time it took to invert a tube five times to mix its contents ("tube flipping"), prior to collecting the immune complexes in a 1 min incubation with protein A/G resin. Following the IP step, mass spectrometry was performed and the SILAC ratios of a subset of the known VCP adaptors were evaluated. For this analysis, we focused our attention on UFD1L-NPLOC4 and the UBX domain adaptors that bind the N-terminal domain and are thought to promote substrate recruitment. The extremely short IPs reduced the efficiency of ^{FLAG}VCP recovery (although less than might be generally assumed; supplemental Fig. S3*B*, S3*C*). Despite the use of extremely short IP intervals, we were able to unambiguously measure SILAC ratios for ^{FLAG}VCP and six of its putative substrate adaptors across all time points. Whereas the SILAC ratios of ^{FLAG}VCP peptides were high, suggesting that protomers within VCP hexamers

did not exchange rapidly, the peptides recovered from VCP adaptors had ratios close to 1 suggesting very rapid equilibration of the heavy and light adaptors with heavy ^{FLAG}VCP (Fig. 3C, supplemental Table S4). A notable exception is ASPSCR1, which was one of the two adaptors that showed strong cofractionation with VCP by SEC (supplemental Fig. S2*A*). Thus, we conclude that the association of ^{FLAG}VCP with most N domain-binding adaptors (and potentially the substrates that bind to those adaptors) is extraordinarily dynamic, and thus what one observes by SEC or in a conventional IP is probably not an accurate reflection of the complexes that exist in the cell.

Although the IP and SEC experiments both pointed to the same conclusion, we had some concern that the epitope tag used for the IP experiments might destabilize the association of ^{FLAG}VCP with its adaptors. To address this issue, we first compared the proteins recovered after the ^{FLAG}VCP IP to those recovered after IP of endogenous untagged VCP with an anti-VCP antibody that binds to a C-terminal epitope on VCP (note that most of the putative substrate-recruitment adaptors bind to the N-terminal domain of VCP, which is far from the location of the antibody epitope in the crystal structure). In this and other experiments (data not shown), we consistently identified more proteins (supplemental Fig. S3*D*, supplemental Table S5), including known VCP adaptors (supplemental Fig. S3*E*), when we used the anti-VCP antibody, suggesting that the N-terminal FLAG tag might indeed reduce the binding of some adaptors. Thus, for future experiments, we employed the anti-VCP antibody.

VCP-adaptor Interaction is Largely Because Of Direct Binding—To evaluate whether untagged VCP also exhibits dynamic association with its adaptors, we needed to develop a method to block association of adaptors with endogenous VCP during the IP step, because it was not possible to perform a conventional PAM-SILAC experiment. Because the epitope recognized by the anti-VCP antibody is in the C-terminal region, we expressed and purified a truncated form of VCP that incorporates the N and D1 domains as well as a linker between the D1 and D2 domains (ND1L). ND1L should bind UFD1L-NPLOC4 and VCP adaptors with a UBX domain (50) but as expected, it did not bind the anti-VCP antibody (Fig. 4*A*). Thus, ND1L added to cell lysates should behave as a passive sponge that soaks up any adaptors that are either not bound to VCP or dissociate from VCP during the IP step, thereby preventing them from rebinding to VCP in the cell lysate. However, ND1L should have no effect on the k_{off} of adaptors that are bound to VCP at the time of cell lysis. It should also not be recovered in the IP step, thereby allowing us to capture a record of the VCP complexes that pre-existed in cells and survived the IP step (Fig. 4*B*). Titration of "light" ND1L into heavy cell lysate prior to IP with anti-VCP for 1 min followed by recovery of immune complexes on protein A/G resin for 5 min reduced the number of proteins recovered (Fig. 4*C*, supplemental Fig. S4), but had no effect on the recovery of heavy VCP (Fig. 4*D*, supplemental Table S6; for this experiment, only C-terminal peptides were counted to rigorously exclude the possibility that they arose from ND1L). Notably, addition of ND1L caused a strong reduction in the recovery of VCP adaptors, with the curious exception of ASPSCR1, and to a lesser extent UBXN2A (Fig. 4*D*). ASPSCR1 was also resistant to exchange in the PAM-SILAC protocol (Fig. 3*C*) and both ASPSCR1 and UBXN2A showed good cofractionation with VCP in the SEC analysis (supplemental Fig. S2*A*). This experiment suggests two important conclusions: (1) ND1L does not dislodge stably bound adaptors from VCP, and (2) most adaptors that bind the N-terminal domain exhibit extremely dynamic association with untagged endogenous VCP and dissociate during a 6 min IP.

In-cell Cross-linking Significantly Increases the Recovery of VCP Adaptors—Given that many VCP-adaptor complexes were extremely prone to dissociation and exchange in cell lysate we reasoned that it is not possible to capture a reliable snapshot of the VCP complexes that existed in a cell using conventional chromatography or IP methods. Therefore, we employed a cross-linking agent to "freeze" VCP complexes, to enable identification of protein interactions that occur in cells. To trap physiological VCP complexes, we added the cross-linking agent DSP to intact cells to stabilize complexes prior to cell lysis. Optimal cross-linking conditions were determined by assessing the formation of high molecular weight (MW) VCP cross-linked complexes as a function of DSP concentration. The lowest concentration of DSP that yielded near-quantitative cross-linking of VCP was 0.8 mM (Fig. 5*A*), and this was therefore employed for subsequent experiments. When IP with anti-VCP was performed for 2 h, most of the cross-linked VCP was recovered in the bound fraction (supplemental Fig. S5). SILAC mass spectrometry analysis revealed that cross-linking with 0.8 mM DSP yielded much higher relative levels of multiple VCP adaptors (with the exception of the slowly exchanging UBXN2A and ASPSCR1, which already bound relatively stably in the absence of cross-linker) than 0.1 mM DSP (Fig. 5*B*). Notably, the adaptor UBXN2B/p37, as well as validated VCP interactors NGLY1, PLAA, and UBE4B were only identified when cells treated with DSP were used for IP with anti-VCP.

Given the superior ability of the cross-linking method to identify VCP adaptors, we performed a global SILAC mass spectrometry analysis in HEK293 cells to identify proteins whose association with VCP was modulated by either the allosteric VCP ATPase inhibitor NMS873 (32) or the proteasome inhibitor MG132. The rationale behind these experiments is that NMS873 might trap VCP in a state that favors binding of certain adaptor proteins and substrates. By contrast, MG132 should prevent the degradation of VCP substrates destined for the proteasome, allowing them to accumulate on VCP. Each SILAC comparison was done in duplicate, and then the mass labels were swapped and the experiment repeated in duplicate again. Comparison of bio-

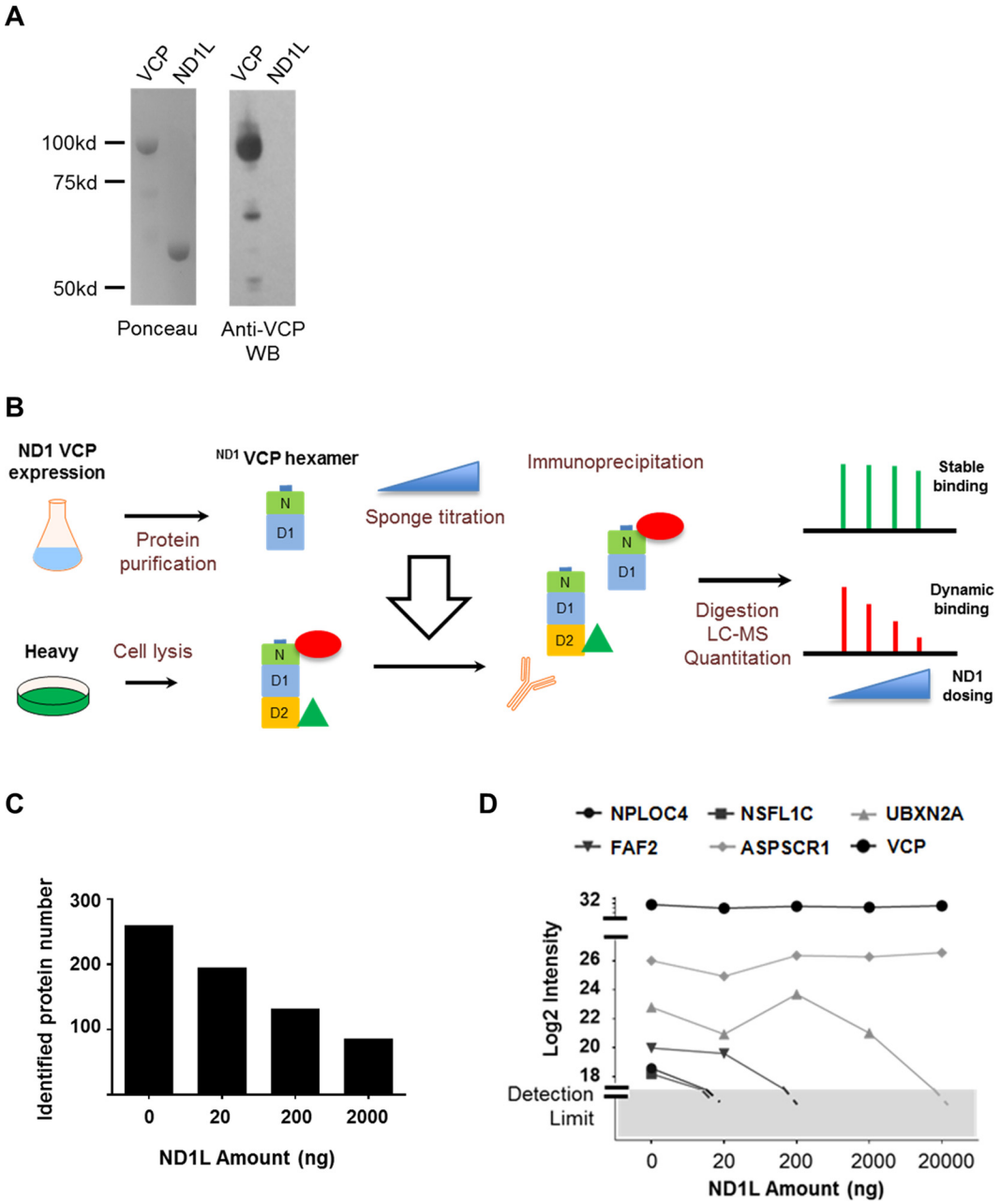

FIG. 4. **VCP adaptors undergo dynamic exchange during IP of untagged endogenous VCP.** *A*, VCP antibody does not bind ND1L. Full-length VCP and the ND1L fragment were fractionated by SDS-PAGE and subjected to Western blotting with anti-VCP. Left panel: Ponceau S staining of the nitrocellulose filter. Right panel: Western blot of the same filter. *B*, Schematic workflow of "Sponge" experiment. *C*, Effect of ND1L competitor on recovery of VCP-interacting proteins. The indicated amounts of purified ND1L were added to 1 milligram of HEK293 cell lysate, which was then subjected to IP for 1 min with anti-VCP followed by 5 min with protein A/G resin prior to mass spectrometry. $n = 1$ for all treatments. *D*, The relative amounts of individual VCP adaptors identified in the experiment in panel B are plotted. Relative protein amounts were estimated by LFQ value from MaxQuant.

logical replicates in each case confirmed the robustness of our methodology (supplemental Figs. S6*A*, S6*B*; for a full list of IDs, see supplemental Table S7). A similar analysis was done on BJ fibroblasts, although label-free mass spectrometry was used instead of SILAC (see supplemental Figs. S6*C*, S6*D* for comparison of replicates and supplemental Table S8 for a full list of IDs). For both experiments, the majority of proteins with >twofold alteration in association with VCP showed increased (as opposed to reduced) binding in the presence of NMS873 or MG132, and many of the proteins that showed enhanced binding in the presence of NMS873 were similarly enriched by MG132 treatment, suggesting that VCP-interacting proteins are often regulated by the proteasome (Fig. 6*A*, 6*B*). In general, these VCP-interacting proteins

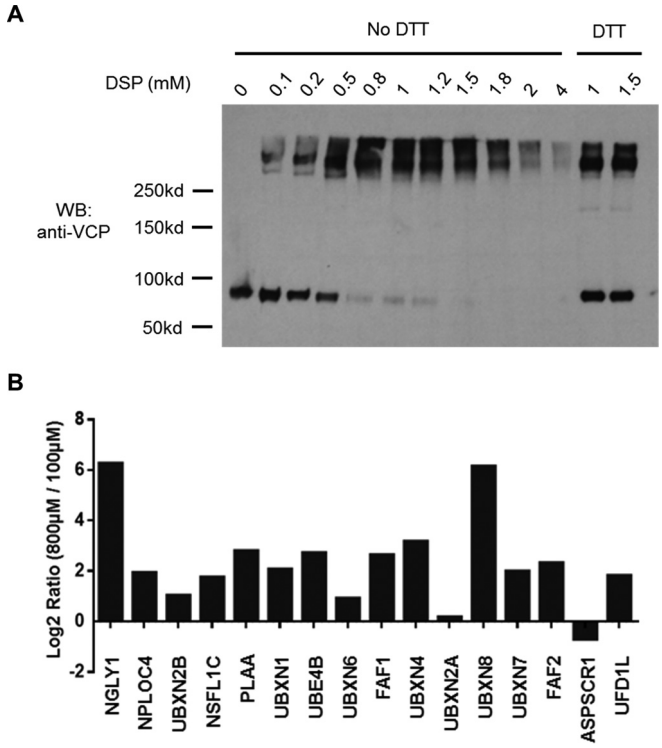

FIG. 5. **The crosslinker DSP stabilizes the interaction of VCP with most of its adaptors.** *A*, DSP was added in the indicated amounts to HEK293 cells in the absence or presence of DTT for 30 min prior to cell lysis. Cross-linking of VCP was evaluated by fractionation of lysates by SDS-PAGE followed by immunoblotting with anti-VCP. *B*, SILAC analysis was performed with heavy—and light—labeled cells treated with 800 μM and 100 μM DSP, respectively. The H/L ratio is reported for the indicated VCP-binding proteins. $n = 1$ for all treatments.

appear to be functionally linked to protein biogenesis and protein quality control, as they are highly enriched for factors involved in nonsense-mediated decay, translation, amino acid metabolism, and cotranslational signal recognition particle (SRP) targeting to membranes (Fig. 6*C*).

Examination of the VCP adaptors revealed that NMS873 had a profound effect on their assembly with VCP: of the 11 N domain-binding substrate adaptors identified in both replicates of the HEK293 experiment, two decreased in amount by at least twofold and five increased in amount by at least twofold upon inhibition of VCP (Fig. 6*D*). Qualitatively similar behavior was observed in the experiment with BJ fibroblasts (Fig. 6*D*). The recovery of increased UBXN7 and FAF2 in association with VCP upon NMS873 treatment is all the more remarkable given that NMS873 treatment reduces the steady-state level of these proteins (23). Inhibition of VCP by NMS873 could stabilize association of some adaptors by at least two conceivable mechanisms. In the first case, NMS873 might stabilize a conformation of VCP that binds more tightly to certain adaptors. In the second case, NMS873 might block degradation of the adaptor or VCP substrates targeted to the UPS, which upon accumulation bind to their cognate adaptors and stabilize their association with VCP. We reasoned that the second hypothesis could be tested by repeating the experiment in the presence of the proteasome inhibitor MG132, which should also block degradation of adaptors and VCP substrates. In this case, we predict that MG132 would enhance adaptor association with VCP. However, we only clearly observed this effect for FAF1 (Fig. 6*D*), and to a significantly lesser extent with UBXN7 (both in HEK293 cells). For the other three adaptors whose VCP association was enhanced by NMS873, MG132 had a relatively negligible effect in both the HEK293 cells and BJ fibroblasts. This suggests that NMS873 might act primarily via a direct conformational effect on VCP.

Bioinformatic Analyses Highlight Similar Responses to VCP Inhibition in Different Cell Types and Emphasize the Benefit of Cross-linking—To evaluate the relative performance of the different approaches taken during the course of this work, we performed comparative bioinformatic analyses of our data sets. Fig. 7*A* charts the behavior of proteins with known VCP binding motifs (UBX, VBM, PUB, VIM, and PUL domains) as well as a handful of other well-studied VCP-interacting proteins in AP-MS experiments performed with and without cross-linking. Some cell type-specific effects are seen (the most dramatic being the strong association of ERAD components AMFR, SYVN1, and DERL2 with VCP in cross-linked BJ cells treated with NMS873), but for the most part the results are similar across cell types, with NMS873 consistently enhancing VCP association of some adaptors while diminishing the association of others. Notably, both NMS873 and MG132 enhanced association of ubiquitin with VCP (annotated here as RPS27A).

Adaptors generally behaved similarly to other adaptors in their subcategory in response to a variety of conditions, including VCP and proteasomal inhibition, as well as during different types of immunoprecipitation. From this, we speculated we might be able to identify candidate substrates of these adaptors by querying for proteins with a similar pattern of variation across the different experiments. Fig. 7*B* (see supplemental Fig. S7 for gene names) provides a graphical representation of the proteins that significantly covaried with each UBX domain adaptor. Some interesting relationships worthy of further investigation were noted, including significant covariation of UBXN4 with proteasome subunits.

To get a better understanding of how different cell types and cell treatments (cross-linking or no cross-linking) compared with each other, we constructed Venn diagrams showing the overlap between different experiments. The upper panel in Fig. 7C shows that 93% of the proteins in HEK293 cells that showed increased binding to VCP upon NMS873 treatment followed by cross-linking, showed the same behavior in similarly treated BJ fibroblasts. By contrast, the overlap between the data sets from cross-linked and noncross-linked HEK293 cells was poor (Fig. 7*C*, lower panel). Given that the percentage of hits that is independently validated (by cross-

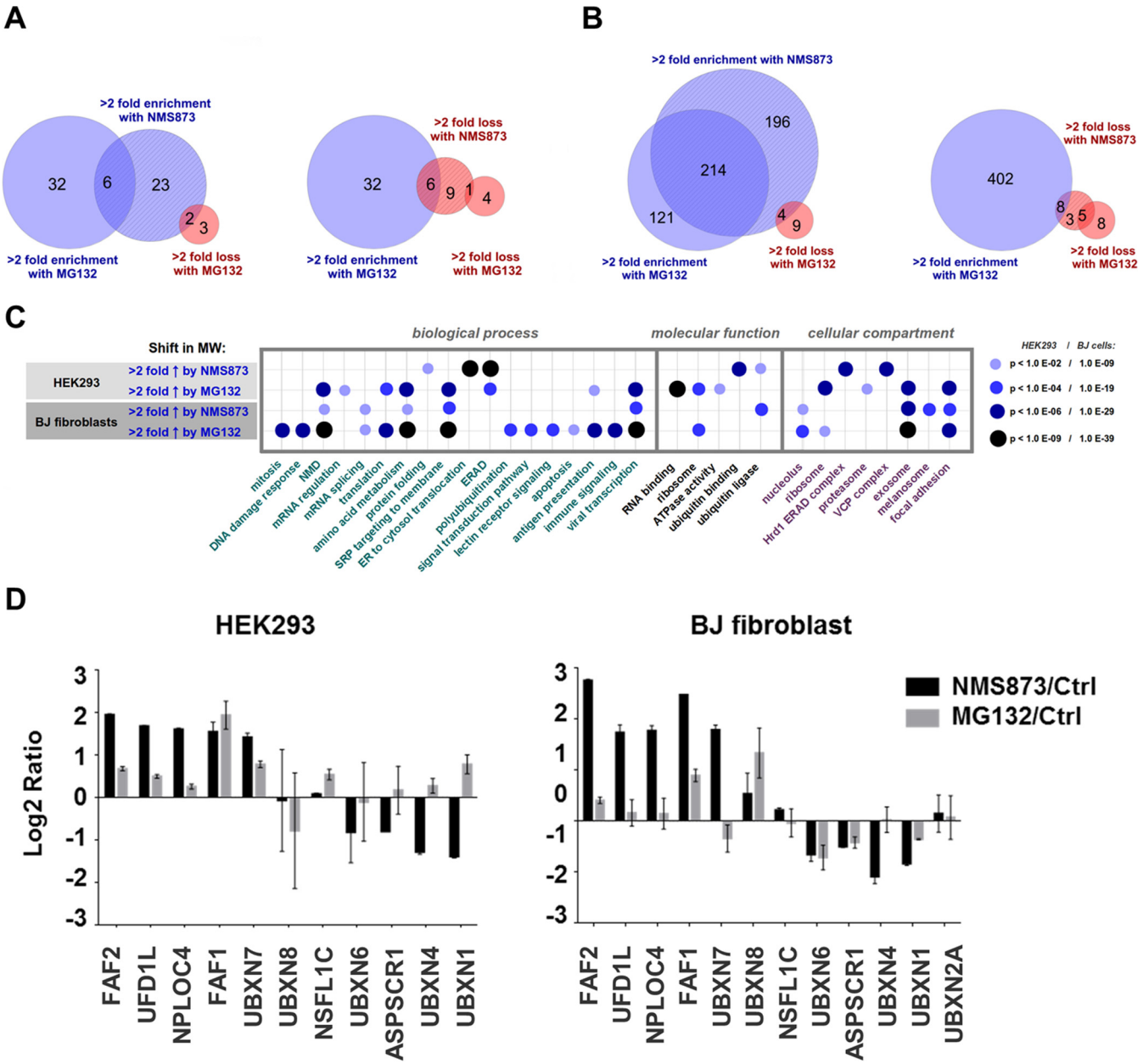

FIG. 6. **Chemical inhibition of VCP modulates its repertoire of associated adaptor proteins.** *A*, Effect of NMS873 and MG132 on VCP-associated proteins in HEK293 cells. Duplicate label-swap SILAC experiments (4 analyses in total) were performed in which cells were either mock-treated or supplemented with 10 μM NMS873 for 6 h, or 10 μM MG132 or vehicle ("control") for 2h. Cells were treated with 800 μM DSP for 30 mins prior to cell lysis, mixing of cell lysates, IP with anti-VCP, and SILAC mass spectrometry analysis. Number of proteins meeting the indicated criteria are depicted. *B*, same as panel *A*, except that BJ fibroblasts were used, all cells were grown in light medium, and relative protein amounts were determined by label-free quantification. *C*, Significant enrichment for gene ontology classes as calculated by PANTHER. All terms with significance below a certain threshold ($p < E^{-02}$ for HEK293 cells; $p < E^{-09}$ for BJ cells) are displayed. *D*, Effect of NMS873 or MG132 treatment on recovery of the indicated adaptor proteins in the VCP IPs from HEK293 cells (left panel) and BJ fibroblasts (right panel) is plotted. Only adaptors detected in both replicates for a given cell type are shown. Error bars represent standard error of the mean ratio, $n = 2$.

referencing with the BioGRID (43) databases) is much higher for the cross-linked data set, many of the additional hits found in the noncross-linked sample may be because of higher nonspecific background. In Fig. 7*D*, the behavior of the 29 proteins that overlap in the top panel of Fig. 7*C* is shown across all experiments performed during the course of this work. Taken together, these data suggest that cross-linking yields data sets with the highest enrichment of validated binding partners (supplemental Table S9). An added benefit of cross-linking is that it enriches for interactions that occur within the cell as opposed to in the lysate, where natural compartment barriers have been breached.

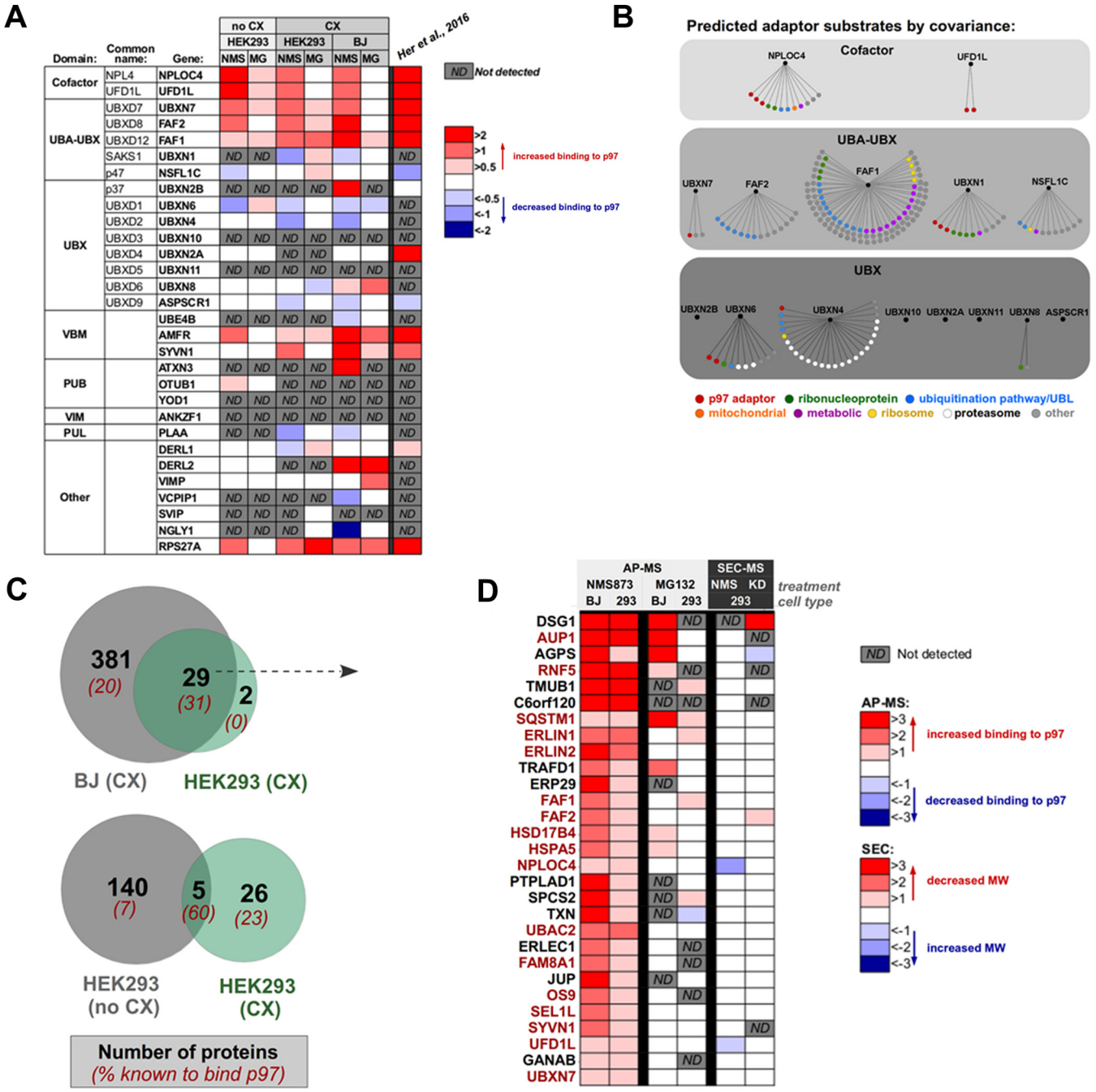

FIG. 7. **Summary of mass spectrometry results.** *A*, Summary of the impact of MG132 or NMS873 treatment on VCP binding proteins highlighted by Her *et al.* (65), in the presence or absence of cross-linking. The final column shows data from (65). The cross-linking data is from Fig. 6, whereas the noncross-linking experiment (supplemental Table S10) was done separately with HEK293 cells using a similar protocol except that label-free quantification was used. *B*, Prediction of potential substrates for UFD1L-NPLOC4 and UBX domain proteins by covariance analyses. Significance of covariance between UBX domain adaptors and all other proteins identified in the AP-MS experiments reported here was calculated through Pearson correlation values. All proteins with $p < 0.05$ are displayed as a colored circle indicating their functional categorization. List of proteins for each adaptor can be found in supplemental Fig. S7 and supplemental Table S10. *C*, Overlap of AP-MS data for cross-linked HEK293 cells with cross-linked BJ fibroblasts and noncross-linked HEK293 cells. Venn diagram depicts overlap of proteins with >twofold enrichment by NMS873 for each cell type/condition. Numbers in black represent absolute number of proteins, whereas numbers in red represent percentage of these proteins reported as binding to VCP (as indexed by BioGRID). The dotted arrow signifies that the 29 proteins that overlap in the upper Venn diagram were used to populate the heatmap in panel *D*. *D*, Proteins with >2 fold enrichment by NMS873 in both HEK293 cells and BJ fibroblasts are depicted, as is the behavior of these same proteins in the SEC-mass spectrometry experiments.

Dynamic Association of NSFL1C with VCP is an Intrinsic Property of the Respective Complexes—Both our SEC and IP mass spectrometry experiments led to the unexpected conclusion that adaptor proteins that are known to function with VCP form extremely dynamic complexes with VCP that undergo rapid dissociation and exchange in cell lysates. We now sought to both validate these findings and place them on a more quantitative footing. To this end, we developed a quantitative FRET assay that allowed us to measure dynamic association of NSFL1C with VCP *in vitro*. Using the crystal structure of NSFL1C bound to the N-domain of VCP as a guide (51), we first mutagenized the C-terminal amino acid (Thr^{370}) of NSFL1C to cysteine, and then reacted the purified recombinant protein with maleimide-TAMRA to generate $NSFL1C^{TAMRA}$ (Fig. 8*A*). For VCP, we used the ybbR tagging method (45) to attach a Cy5 tag at its N terminus (^{Cy5}VCP; Fig. 8*A*). Upon mixing $NSFL1C^{TAMRA}$ and ^{Cy5}VCP and exciting with 540 nm light, we observed a significant reduction in TAMRA fluorescence coupled to an increase in Cy5 emission (Fig. 8*B*). This FRET signal was because of specific interaction of $NSFL1C^{TAMRA}$ and ^{Cy5}VCP, because it was competed by addition of excess unlabeled VCP (Fig. 8*B*). By titrating ^{Cy5}VCP, we estimated a K_d of 65 nM for interaction of the two proteins in the absence of nucleotide (Fig. 8*C* and Table I). This affinity is ~10-fold tighter than what was reported from isothermal titration calorimetry studies (52, 53), but is close to the affinity measured in a pair of surface plasmon resonance (SPR) studies (20–31 nM) (50, 54). However, there are significant problems with measuring NSFL1C-VCP interactions by SPR because of the oligomeric nature of both proteins. In addition, none of the studies cited above addressed the crucial issue of the dynamics of NSFL1C-VCP interaction. To investigate binding dynamics, we measured the k_{on} for complex formation and k_{off} for complex dissociation in the absence of nucleotide ("apo") or in the presence of ADP or ATPγS with and without VCP inhibitors. Examples of k_{off} and k_{on} measurements in the absence of nucleotide are shown in Figs. 8*D* and 8*E*, respectively, and a plot of k_{obs} *versus* [^{Cy5}VCP] that was used to estimate k_{on} is shown in Fig. 8*F*. As shown in Table I, k_{on} values were essentially invariant, ranging from 8–11 $\times$ 10^7 M^{-1} sec^{-1} regardless of nucleotide state. Meanwhile, k_{off} showed slightly more variation, ranging from 2.5 s^{-1} in the presence of ATP and NMS873 to 9.5 s^{-1} in the presence of ADP. Consistent with the lack of an effect of NMS873 on co-IP of NSFL1C with VCP from lysates of BJ cells treated with DSP (Fig. 6*D*), addition of NMS873 in the presence of ATP had less than a twofold effect on k_{off} (Table I). These results confirm that purified $NSFL1C^{TAMRA}$ exhibited extremely dynamic association with purified ^{Cy5}VCP in accordance with the behavior of these proteins in HEK293 cell extracts, and that their association was relatively insensitive to modulation by NMS873.

DISCUSSION

We set out in this study with the goal of using size exclusion chromatography coupled to mass spectrometry to characterize VCP-adaptor interactions and identify new VCP-interacting proteins. However, in the course of carrying out these experiments, we made the surprising finding that VCP shows little or no cofractionation with adaptors that are well-validated to bind VCP. Similar results were observed in conventional immunoprecipitation mass spectrometry experiments, in which SILAC was used to quantify the degree to which VCP-binding proteins undergo exchange during purification. Characterization of the interaction between VCP and its adaptors has led to two important conclusions. First, under unperturbed conditions, VCP dissociates rapidly from all adaptors in cell lysate except ASPSCR1 and probably UBXN2A. We were able to reproduce this finding using purified VCP and NSFL1C, indicating that rapid exchange is likely to be an intrinsic property of VCP-adaptor interactions. Second, inhibition of VCP ATPase activity with the allosteric inhibitor NMS873 has markedly distinct effects on the interaction of different adaptors with VCP. Each of these findings has significant implications, which are discussed in more detail in the following paragraphs.

A Cautionary Note for Analysis of VCP-interacting Proteins—Because the interaction of VCP with its adaptors is so dynamic, lists of VCP-interacting proteins obtained through conventional immunoprecipitation protocols (21, 23, 28) are most likely dominated by proteins that formed interactions with VCP in cell lysate. Whereas many of these interactions are nonetheless likely to be physiological, some of them might not be, because of the loss of compartmentation and other forms of regulation that accompanies cell lysis. To some extent adaptor dynamics can be suppressed by NMS873 as discussed in the next section, but it must be appreciated that NMS873 has differential effects on adaptors and thus does not preserve the natural state that existed in cells. The only strategy we have identified that is likely to adequately suppress adaptor exchange is to treat cells with cross-linking agents prior to cell lysis and IP, but that can carry its own risks. In the absence of cross-linking, few proteins were identified that were also found in our cross-linking data–set, and the majority of these proteins have not been reported to bind VCP (Fig. 7*C*, full list can be found in supplemental Table S11). Therefore, we suspect that VCP-interacting proteins recovered in the absence of cross-linking may not accurately represent the physiological associations of VCP. We did not address whether association of proteins with VCP adaptors is also subject to the same dynamic behavior documented here for VCP-adaptor interactions, but this possibility should be borne in mind.

An analysis of the effects of NMS873 on VCP-interacting proteins appeared while we were finalizing our manuscript (55). Although their mass spectrometry findings are generally

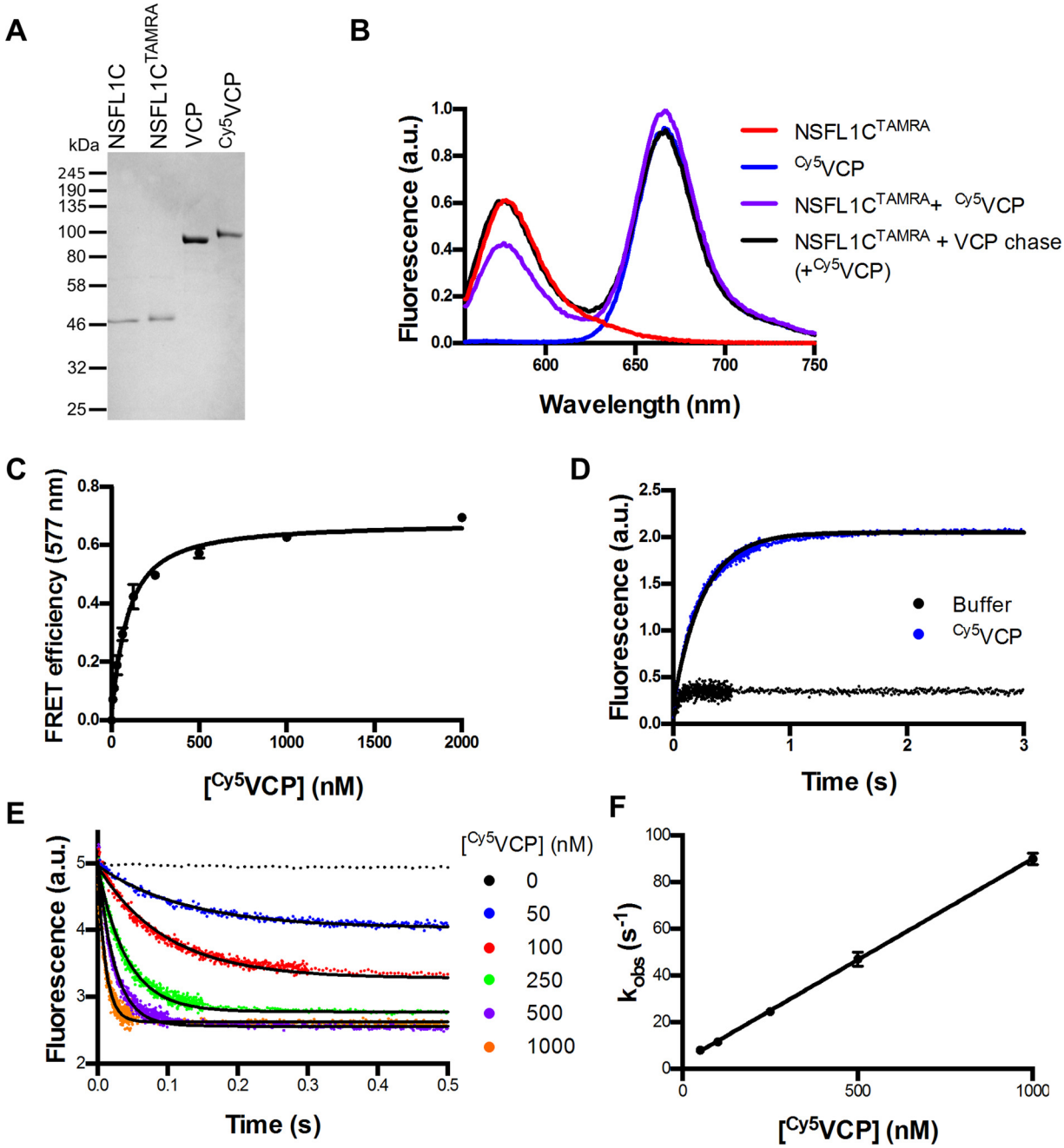

FIG. 8. **Biochemical characterization of VCP-adaptor interactions.** *A*, SDS-PAGE gel of purified recombinant proteins used in this study. *B*, Fluorescence emission spectra of 16.7 nM NSFL1C^{TAMRA} trimer, 83.3 nM ^{Cy5}VCP hexamer, and a mixture excited at 540 nm shows a ~20% loss of TAMRA donor fluorescence in the presence of ^{Cy5}VCP. Loss of fluorescence is prevented by preincubation of NSFL1C^{TAMRA} with 833 nM unlabeled VCP hexamer. *C*, Equilibrium titration of 50 nM NSFL1C^{TAMRA} trimer with ^{Cy5}VCP hexamer. Fit to a quadratic binding equation yields a K_D of 65 ± 7 nM. Error bars represent ± S.D., with $n = 3$. *D*, Change in donor fluorescence of 50 nM NSFL1C^{TAMRA} trimer preincubated with 300 nM ^{Cy5}VCP hexamer upon addition of 3 μM unlabeled VCP hexamer in the absence of nucleotide. Curve was fit to a single exponential to give k_{off} of 4.04 s^{-1}. *E*, Change in donor fluorescence of 50 nM NSFL1C^{TAMRA} trimer upon addition of ^{Cy5}VCP hexamer at various concentrations in the absence of nucleotide. Curves were fit to a single exponential. *F*, Exponential fits measured in panel E plotted against the concentration of ^{Cy5}VCP hexamer. Linear slope gives k_{on} of 8.68 × 10^7 $M^{-1}s^{-1}$. Error bars represent ± S.D., with n ≥ 5.

consistent with our own (see Fig. 7*A* for a comparison), their work focused primarily on mechanisms of VCP resistance to NMS873 and consequently there are several important differences with the work reported here. First, their analyses were performed exclusively under native (*i.e.* noncross-linked) conditions that favor interactions formed in cell lysate. Second, our coverage of known VCP interactors was substantially more comprehensive. Finally, Her *et al.* did not evaluate the

TABLE I
Kinetic and equilibrium binding constants for NSFL1C^{TAMRA} and ^{Cy5}VCP

Nucleotide state	Inhibitor	K_D (eq) (nM)	k_{on} ($\times 10^7$ M^{-1}s^{-1})	k_{off} (s^{-1})	K_D (k_{off}/k_{on}) (nM)
Apo	-	65 ± 7	8.68 ± 0.09	4.04 ± 0.09	47
ATPγS	-	n.d.	10.5 ± 0.1	3.30 ± 0.02	31
ADP	-	n.d.	8.30 ± 0.07	9.50 ± 0.08	114
Apo	CB-5083	n.d.	8.0 ± 0.1	4.80 ± 0.03	60
ATP	NMS-873	n.d.	11.01 ± 0.01	2.50 ± 0.03	28

extent of VCP-adaptor exchange in cell lysate or with purified proteins.

Dynamics of VCP-adaptor Interactions—The extremely rapid off-rates that we documented for NSFL1C-VCP complexes pose an interesting question: can VCP-adaptor complexes adequately perform their tasks in cells? VCP has been reported to have a turnover rate ranging from 0.75–5.2 ATP per second per hexamer (38, 56–58). Thus, each protomer turns over less than 1 ATP per second. By comparison, the slowest k_{off} that we measured for uninhibited VCP-NSFL1C complexes is 3.3 s^{-1}. Comparing these numbers suggests that, at most, 1 or 2 ATP is hydrolyzed per hexamer during the lifespan of a VCP-NSFL1C complex, and this is likely to be a maximal estimate because NSFL1C moderately slows down ATP hydrolysis by VCP (54, 59). It seems unlikely that this level of ATP hydrolysis would be sufficient to sustain the proposed segregase function of VCP. We speculate that there are mechanisms that modulate the lifespan of VCP-adaptor complexes. Consistent with this idea, NSFL1C forms a tight complex with VCP and copurifies with it from rat liver extracts (60), whereas we did not observe comigration of these proteins during SEC of HEK293 cell extracts. Thus, there may exist factors in liver cells that stabilize VCP-NSFL1C complexes. This could include covalent modifications on VCP, of which many have been reported (61), covalent modifications on the adaptor (62), or engagement of substrate by the adaptor.

In contrast to the behavior of most adaptors, ASPSCR1 (also known as UBXD9, TUG, or ASPL) exhibited relatively stable binding to VCP in both the IP and SEC protocols. It was reported previously that the vast majority of ASPSCR1 is bound to VCP (consistent with our results in the SEC experiment, supplemental Fig. S2*A*), and disassembles VCP hexamers into monomers (63). However, the physiological significance of this remodeling was not determined. UBXN2A exhibited a similar behavior to ASPSCR1, but in addition its expression appeared to depend on the presence of VCP (supplemental Fig. S2*A*), suggesting that UBXN2A stability may be dependent upon its assembly with VCP. Interestingly, although ASPSCR1 has been linked to GLUT4 trafficking (64) and UBXN2A to mortalin (65) and nicotinic acetylcholine receptors (66), neither protein has been shown to link specific substrates to VCP. Given the distinct VCP binding dynamics and stoichiometries displayed by UBXN2A and ASPSCR1, these proteins may not function as substrate adaptors but instead may sequester or recycle VCP hexamers.

Effects of ATPase Inhibitors on VCP-adaptor Association—The reversible, competitive VCP ATPase inhibitor CB-5083 is in clinical development for treatment of cancer. We still know relatively little about the full range of physiological functions and regulation of VCP, which creates a challenge for thinking about the disease settings in which VCP inhibition is likely to be most efficacious. From this perspective, it is of interest that the reversible, allosteric VCP ATPase inhibitor NMS873 (32) exhibited strong differential effects on the association of adaptors with VCP. An intriguing idea is that, in principal, the reciprocal should also be true—adaptors whose binding to VCP is stabilized by an inhibitor should also stabilize binding of the inhibitor to VCP. This raises the possibility that different VCP-adaptor complexes might show differential sensitivity to small molecule inhibition, which has been suggested in prior studies with NSFL1C (38). Preferential inhibition of particular VCP-adaptor complexes could be an effective strategy to focus inhibition on VCP complexes that are of particular importance to the survival of cancer cells that have constitutively high levels of unfolded protein response (67).

Acknowledgments—We thank the Shu-ou Shan lab for Sfp plasmid, T.F. Chou for full-length human VCP in pET15, and S. Bulfer and M. Arkin for ND1L construct. We thank Shu-ou Shan and members of the Shan lab for helpful discussion on the FRET assay, Xun Wang for assistance of VCP tagging by CRISPR technique, and R. Verma for helpful suggestions and comments on the manuscript. We also thank Tanya Porras-Yakushi for help in editing the manuscript for clarity, Annie Moradian and Roxana Eggleston-Rangel for mass spectrometry support and Michael J. Sweredoski for bioinformatics assistance.

* This work was supported by the Gordon and Betty Moore Foundation, through Grant GBMF775, the Beckman Institute and the NIH through Grant 1S10RR029594 (to SH). J.M.R. was supported by a postdoctoral fellowship from NIH (F32 GM112308-03). R.J.D. is an Investigator of the Howard Hughes Medical Institute and this work was funded by HHMI. E.E.B. is supported by an NIH Training Grant (T32 GM007616). The content is solely the responsibility of the authors and does not necessarily represent the official views of the National Institutes of Health.

S This article contains supplemental material.

§§ To whom correspondence should be addressed: Division of Biology, California Institute of Technology, 1200 E. California Blvd., Pasadena, CA. E-mail: deshaies@caltech.edu.

Additional Information: Supplemental data set containing 7 Figs. and 11 Tables. The mass spectrometry proteomics data for supplemental Table S1, S2, and S5 have been deposited to the Chorus Project (chorusproject.org) with the project identifier 1068. Other mass spectrometry proteomics data have been deposited to ProteomeXchange

Consortium (http://proteomecentral.proteomexchange.org) via the PRIDE partner repository (68) with the data set identifier PXD004105.

REFERENCES

1. Balch, W. E., Morimoto, R. I., Dillin, A., and Kelly, J. W. (2008) Adapting proteostasis for disease intervention. *Science* **319,** 916–919
2. Bukau, B., Weissman, J., and Horwich, A. (2006) Molecular chaperones and protein quality control. *Cell* **125,** 443–451
3. Doyle, S. M., Genest, O., and Wickner, S. (2013) Protein rescue from aggregates by powerful molecular chaperone machines. *Nat. Rev. Mol. Cell Biol.* **14,** 617–629
4. Goldberg, A. L. (2003) Protein degradation and protection against misfolded or damaged proteins. *Nature* **426,** 895–899
5. Luo, J., Solimini, N. L., and Elledge, S. J. (2009) Principles of cancer therapy: oncogene and non-oncogene addiction. *Cell* **136,** 823–837
6. Santaguida, S., and Amon, A. (2015) Short- and long-term effects of chromosome mis-segregation and aneuploidy. *Nat. Rev. Mol. Cell Biol.* **16,** 473–485
7. Arias, E., and Cuervo, A. M. (2011) Chaperone-mediated autophagy in protein quality control. *Curr. Opin. Cell Biol.* **23,** 184–189
8. Deshaies, R. J. (2014) Proteotoxic crisis, the ubiquitin-proteasome system, and cancer therapy. *BMC Biol.* **12,** 94
9. Teicher, B. A., and Anderson, K. C. (2015) CCR 20th anniversary commentary: In the beginning, there was PS-341. *Clin. Cancer Res.* **21,** 939–941
10. Verma, R., Oania, R. S., Kolawa, N. J., and Deshaies, R. J. (2013) Cdc48/p97 promotes degradation of aberrant nascent polypeptides bound to the ribosome. *eLife* **2,** e00308
11. Brandman, O., Stewart-Ornstein, J., Wong, D., Larson, A., Williams, C. C., Li, G. W., Zhou, S., King, D., Shen, P. S., Weibezahn, J., Dunn, J. G., Rouskin, S., Inada, T., Frost, A., and Weissman, J. S. (2012) A ribosome-bound quality control complex triggers degradation of nascent peptides and signals translation stress. *Cell* **151,** 1042–1054
12. Defenouillere, Q., Yao, Y., Mouaikel, J., Namane, A., Galopier, A., Decourty, L., Doyen, A., Malabat, C., Saveanu, C., Jacquier, A., and Fromont-Racine, M. (2013) Cdc48-associated complex bound to 60S particles is required for the clearance of aberrant translation products. *Proc. Natl. Acad. Sci. U.S.A.* **110,** 5046–5051
13. Taylor, E. B., and Rutter, J. (2011) Mitochondrial quality control by the ubiquitin-proteasome system. *Biochem. Soc. Trans.* **39,** 1509–1513
14. Ye, Y., Meyer, H. H., and Rapoport, T. A. (2001) The AAA ATPase Cdc48/p97 and its partners transport proteins from the ER into the cytosol. *Nature* **414,** 652–656
15. Meyer, H., and Weihl, C. C. (2014) The VCP/p97 system at a glance: connecting cellular function to disease pathogenesis. *J. Cell Sci.* **127,** 3877–3883
16. Medicherla, B., and Goldberg, A. L. (2008) Heat shock and oxygen radicals stimulate ubiquitin-dependent degradation mainly of newly synthesized proteins. *J. Cell Biol.* **182,** 663–673
17. Ju, J. S., Fuentealba, R. A., Miller, S. E., Jackson, E., Piwnica-Worms, D., Baloh, R. H., and Weihl, C. C. (2009) Valosin-containing protein (VCP) is required for autophagy and is disrupted in VCP disease. *J. Cell Biol.* **187,** 875–888
18. Tresse, E., Salomons, F. A., Vesa, J., Bott, L. C., Kimonis, V., Yao, T. P., Dantuma, N. P., and Taylor, J. P. (2010) VCP/p97 is essential for maturation of ubiquitin-containing autophagosomes and this function is impaired by mutations that cause IBMPFD. *Autophagy* **6,** 217–227
19. Buchan, J. R., Kolaitis, R. M., Taylor, J. P., and Parker, R. (2013) Eukaryotic stress granules are cleared by autophagy and Cdc48/VCP function. *Cell* **153,** 1461–1474
20. Ju, J. S., Miller, S. E., Hanson, P. I., and Weihl, C. C. (2008) Impaired protein aggregate handling and clearance underlie the pathogenesis of p97/VCP-associated disease. *J. Biol. Chem.* **283,** 30289–30299
21. Alexandru, G., Graumann, J., Smith, G. T., Kolawa, N. J., Fang, R., and Deshaies, R. J. (2008) UBXD7 binds multiple ubiquitin ligases and implicates p97 in HIF1alpha turnover. *Cell* **134,** 804–816
22. Buchberger, A., Schindelin, H., and Hanzelmann, P. (2015) Control of p97 function by cofactor binding. *FEBS Lett.* **589,** 2578–2589
23. Raman, M., Sergeev, M., Garnaas, M., Lydeard, J. R., Huttlin, E. L., Goessling, W., Shah, J. V., and Harper, J. W. (2015) Systematic proteomics of the VCP-UBXD adaptor network identifies a role for UBXN10 in regulating ciliogenesis. *Nat. Cell Biol.* **17,** 1356–1369
24. Schuberth, C., and Buchberger, A. (2008) UBX domain proteins: major regulators of the AAA ATPase Cdc48/p97. *Cell Mol. Life Sci.* **65,** 2360–2371
25. Elsasser, S., and Finley, D. (2005) Delivery of ubiquitinated substrates to protein-unfolding machines. *Nat. Cell Biol.* **7,** 742–749
26. Verma, R., Oania, R., Fang, R., Smith, G. T., and Deshaies, R. J. (2011) Cdc48/p97 mediates UV-dependent turnover of RNA Pol II. *Mol. Cell* **41,** 82–92
27. Riemer, A., Dobrynin, G., Dressler, A., Bremer, S., Soni, A., Iliakis, G., and Meyer, H. (2014) The p97-Ufd1-Npl4 ATPase complex ensures robustness of the G2/M checkpoint by facilitating CDC25A degradation. *Cell Cycle* **13,** 919–927
28. Ritz, D., Vuk, M., Kirchner, P., Bug, M., Schutz, S., Hayer, A., Bremer, S., Lusk, C., Baloh, R. H., Lee, H., Glatter, T., Gstaiger, M., Aebersold, R., Weihl, C. C., and Meyer, H. (2011) Endolysosomal sorting of ubiquitylated caveolin-1 is regulated by VCP and UBXD1 and impaired by VCP disease mutations. *Nat. Cell Biol.* **13,** 1116–1123
29. He, J., Zhu, Q., Wani, G., Sharma, N., and Wani, A. A. (2016) VCP/p97 Segregase Mediates Proteolytic Processing of CSB in Damaged Chromatin. *J. Biol. Chem.* **291,** 7396–708
30. Jentsch, S., and Rumpf, S. (2007) Cdc48 (p97): a "molecular gearbox" in the ubiquitin pathway? *Trends Biochem. Sci.* **32,** 6–11
31. Chou, T. F., Brown, S. J., Minond, D., Nordin, B. E., Li, K., Jones, A. C., Chase, P., Porubsky, P. R., Stoltz, B. M., Schoenen, F. J., Patricelli, M. P., Hodder, P., Rosen, H., and Deshaies, R. J. (2011) A reversible inhibitor of the AAA ATPase p97, DBeQ, impairs both ubiquitin-dependent and autophagic protein clearance pathways. *Proc. Natl. Acad. Sci. U.S.A.* **108,** 4834–4839
32. Magnaghi, P., D'Alessio, R., Valsasina, B., Avanzi, N., Rizzi, S., Asa, D., Gasparri, F., Cozzi, L., Cucchi, U., Orrenius, C., Polucci, P., Ballinari, D., Perrera, C., Leone, A., Cervi, G., Casale, E., Xiao, Y., Wong, C., Anderson, D. J., Galvani, A., Donati, D., O'Brien, T., Jackson, P. K., and Isacchi, A. (2013) Covalent and allosteric inhibitors of the ATPase VCP/p97 induce cancer cell death. *Nat. Chem. Biol.* **9,** 548–556
33. Acharya, P., Liao, M., Engel, J. C., and Correia, M. A. (2011) Liver cytochrome P450 3A endoplasmic reticulum-associated degradation: a major role for the p97 AAA ATPase in cytochrome p450 3A extraction into the cytosol. *J. Biol. Chem.* **286,** 3815–3828
34. Piccirillo, R., and Goldberg, A. L. (2012) The p97/VCP ATPase is critical in muscle atrophy and the accelerated degradation of muscle proteins. *EMBO J.* **31,** 3334–3350
35. Chou, T. F., Li, K., Frankowski, K. J., Schoenen, F. J., and Deshaies, R. J. (2013) Structure-activity relationship study reveals ML240 and ML241 as potent and selective inhibitors of p97 ATPase. *Chem. Med. Chem.* **8,** 297–312
36. Zhou, H. J., Wang, J., Yao, B., Wong, S., Djakovic, S., Kumar, B., Rice, J., Valle, E., Soriano, F., Menon, M. K., Madriaga, A., Kiss von Soly, S., Kumar, A., Parlati, F., Yakes, F. M., Shawver, L., Le Moigne, R., Anderson, D. J., Rolfe, M., and Wustrow, D. (2015) Discovery of a First-in-Class, Potent, Selective, and Orally Bioavailable Inhibitor of the p97 AAA ATPase (CB-5083). *J. Med. Chem.* **58,** 9480–9497
37. Anderson, D. J., Le Moigne, R., Djakovic, S., Kumar, B., Rice, J., Wong, S., Wang, J., Yao, B., Valle, E., Kiss von Soly, S., Madriaga, A., Soriano, F., Menon, M. K., Wu, Z. Y., Kampmann, M., Chen, Y., Weissman, J. S., Aftab, B. T., Yakes, F. M., Shawver, L., Zhou, H. J., Wustrow, D., and Rolfe, M. (2015) Targeting the AAA ATPase p97 as an Approach to Treat Cancer through Disruption of Protein Homeostasis. *Cancer Cell* **28,** 653–665
38. Chou, T. F., Bulfer, S. L., Weihl, C. C., Li, K., Lis, L. G., Walters, M. A., Schoenen, F. J., Lin, H. J., Deshaies, R. J., and Arkin, M. R. (2014) Specific Inhibition of p97/VCP ATPase and Kinetic Analysis Demonstrate Interaction between D1 and D2 ATPase domains. *J. Mol. Biol.* **426,** 2886–2899
39. Yu, C. C., Yang, J. C., Chang, Y. C., Chuang, J. G., Lin, C. W., Wu, M. S., and Chow, L. P. (2013) VCP phosphorylation-dependent interaction partners prevent apoptosis in Helicobacter pylori-infected gastric epithelial cells. *PLoS ONE* **8,** e55724
40. Szymczak, A. L., Workman, C. J., Wang, Y., Vignali, K. M., Dilioglou, S., Vanin, E. F., and Vignali, D. A. (2004) Correction of multi-gene deficiency in vivo using a single 'self-cleaving' 2A peptide-based retroviral vector. *Nat. Biotechnol.* **22,** 589–594

41. Cong, L., Ran, F. A., Cox, D., Lin, S., Barretto, R., Habib, N., Hsu, P. D., Wu, X., Jiang, W., Marraffini, L. A., and Zhang, F. (2013) Multiplex genome engineering using CRISPR/Cas systems. *Science* **339,** 819–823
42. Ran, F. A., Hsu, P. D., Wright, J., Agarwala, V., Scott, D. A., and Zhang, F. (2013) Genome engineering using the CRISPR-Cas9 system. *Nat. Protocols* **8,** 2281–2308
43. Stark, C., Breitkreutz, B. J., Reguly, T., Boucher, L., Breitkreutz, A., and Tyers, M. (2006) BioGRID: a general repository for interaction datasets. *Nucleic Acids Res.* **34,** D535–D539
44. Bruderer, R. M., Brasseur, C., and Meyer, H. H. (2004) The AAA ATPase p97/VCP interacts with its alternative co-factors, Ufd1-Npl4 and p47, through a common bipartite binding mechanism. *J. Biol. Chem.* **279,** 49609–49616
45. Yin, J., Lin, A. J., Golan, D. E., and Walsh, C. T. (2006) Site-specific protein labeling by Sfp phosphopantetheinyl transferase. *Nat. Protocols* **1,** 280–285
46. Kirkwood, K. J., Ahmad, Y., Larance, M., and Lamond, A. I. (2013) Characterization of native protein complexes and protein isoform variation using size-fractionation-based quantitative proteomics. *Mol. Cell. Proteomics* **12,** 3851–3873
47. Shalem, O., Sanjana, N. E., Hartenian, E., Shi, X., Scott, D. A., Mikkelsen, T. S., Heckl, D., Ebert, B. L., Root, D. E., Doench, J. G., and Zhang, F. (2014) Genome-scale CRISPR-Cas9 knockout screening in human cells. *Science* **343,** 84–87
48. Wang, X., and Huang, L. (2008) Identifying dynamic interactors of protein complexes by quantitative mass spectrometry. *Mol. Cell. Proteomics* **7,** 46–57
49. Mann, M. (2006) Functional and quantitative proteomics using SILAC. *Nat. Rev. Mol. Cell Biol.* **7,** 952–958
50. Chia, W. S., Chia, D. X., Rao, F., Bar Nun, S., and Geifman Shochat, S. (2012) ATP binding to p97/VCP D1 domain regulates selective recruitment of adaptors to its proximal N-domain. *PLoS ONE* **7,** e50490
51. Dreveny, I., Kondo, H., Uchiyama, K., Shaw, A., Zhang, X., and Freemont, P. S. (2004) Structural basis of the interaction between the AAA ATPase p97/VCP and its adaptor protein p47. *EMBO J.* **23,** 1030–1039
52. Beuron, F., Dreveny, I., Yuan, X., Pye, V. E., McKeown, C., Briggs, L. C., Cliff, M. J., Kaneko, Y., Wallis, R., Isaacson, R. L., Ladbury, J. E., Matthews, S. J., Kondo, H., Zhang, X., and Freemont, P. S. (2006) Conformational changes in the AAA ATPase p97-p47 adaptor complex. *EMBO J.* **25,** 1967–1976
53. Hanzelmann, P., Buchberger, A., and Schindelin, H. (2011) Hierarchical binding of cofactors to the AAA ATPase p97. *Structure* **19,** 833–843
54. Zhang, X., Gui, L., Zhang, X., Bulfer, S. L., Sanghez, V., Wong, D. E., Lee, Y., Lehmann, L., Lee, J. S., Shih, P. Y., Lin, H. J., Iacovino, M., Weihl, C. C., Arkin, M. R., Wang, Y., and Chou, T. F. (2015) Altered cofactor regulation with disease-associated p97/VCP mutations. *Proc. Natl. Acad. Sci. U.S.A.* **112,** E1705–E1714
55. Her, N. G., Toth, J. I., Ma, C. T., Wei, Y., Motamedchaboki, K., Sergienko, E., and Petroski, M. D. (2016) p97 Composition Changes Caused by Allosteric Inhibition Are Suppressed by an On-Target Mechanism that Increases the Enzyme's ATPase Activity. *Cell Chem. Biol.* **23,** 517–528
56. Song, C., Wang, Q., and Li, C. C. (2003) ATPase activity of p97-valosin-containing protein (VCP). D2 mediates the major enzyme activity, and D1 contributes to the heat-induced activity. *J. Biol. Chem.* **278,** 3648–3655
57. Niwa, H., Ewens, C. A., Tsang, C., Yeung, H. O., Zhang, X., and Freemont, P. S. (2012) The role of the N-domain in the ATPase activity of the mammalian AAA ATPase p97/VCP. *J. Biol. Chem.* **287,** 8561–8570
58. DeLaBarre, B., Christianson, J. C., Kopito, R. R., and Brunger, A. T. (2006) Central pore residues mediate the p97/VCP activity required for ERAD. *Mol. Cell* **22,** 451–462
59. Meyer, H. H., Kondo, H., and Warren, G. (1998) The p47 co-factor regulates the ATPase activity of the membrane fusion protein, p97. *FEBS Lett.* **437,** 255–257
60. Kondo, H., Rabouille, C., Newman, R., Levine, T. P., Pappin, D., Freemont, P., and Warren, G. (1997) p47 is a cofactor for p97-mediated membrane fusion. *Nature* **388,** 75–78
61. Mori-Konya, C., Kato, N., Maeda, R., Yasuda, K., Higashimae, N., Noguchi, M., Koike, M., Kimura, Y., Ohizumi, H., Hori, S., and Kakizuka, A. (2009) p97/valosin-containing protein (VCP) is highly modulated by phosphorylation and acetylation. *Genes Cells* **14,** 483–497
62. Uchiyama, K., Jokitalo, E., Lindman, M., Jackman, M., Kano, F., Murata, M., Zhang, X., and Kondo, H. (2003) The localization and phosphorylation of p47 are important for Golgi disassembly-assembly during the cell cycle. *J. Cell Biol.* **161,** 1067–1079
63. Orme, C. M., and Bogan, J. S. (2012) The ubiquitin regulatory X (UBX) domain-containing protein TUG regulates the p97 ATPase and resides at the endoplasmic reticulum-golgi intermediate compartment. *J. Biol. Chem.* **287,** 6679–6692
64. Belman, J. P., Habtemichael, E. N., and Bogan, J. S. (2014) A proteolytic pathway that controls glucose uptake in fat and muscle. *Rev. Endocr. Metab. Disord.* **15,** 55–66
65. Sane, S., Abdullah, A., Boudreau, D. A., Autenried, R. K., Gupta, B. K., Wang, X., Wang, H., Schlenker, E. H., Zhang, D., Telleria, C., Huang, L., Chauhan, S. C., and Rezvani, K. (2014) Ubiquitin-like (UBX)-domain-containing protein, UBXN2A, promotes cell death by interfering with the p53-Mortalin interactions in colon cancer cells. *Cell Death Dis.* **5,** e1118
66. Rezvani, K., Teng, Y., Pan, Y., Dani, J. A., Lindstrom, J., Garcia Gras, E. A., McIntosh, J. M., and De Biasi, M. (2009) UBXD4, a UBX-containing protein, regulates the cell surface number and stability of alpha3-containing nicotinic acetylcholine receptors. *J. Neurosci.* **29,** 6883–6896
67. Chou, T. F., and Deshaies, R. J. (2011) Development of p97 AAA ATPase inhibitors. *Autophagy* **7,** 1091–1092
68. Vizcaino, J. A., Cote, R. G., Csordas, A., Dianes, J. A., Fabregat, A., Foster, J. M., Griss, J., Alpi, E., Birim, M., Contell, J., O'Kelly, G., Schoenegger, A., Ovelleiro, D., Perez-Riverol, Y., Reisinger, F., Rios, D., Wang, R., and Hermjakob, H. (2013) The PRoteomics IDEntifications (PRIDE) database and associated tools: status in 2013. *Nucleic Acids Res.* **41,** D1063–D1069